SPINE Volume 34, Number 2, pp 115–120
©2009, Lippincott Williams & Wilkins

The Efficacy of Prostaglandin E1 Derivative in Patients With Lumbar Spinal Stenosis

Ko Matsudaira, MD,* Atsushi Seichi, MD,* Junichi Kunogi, MD,† Takashi Yamazaki, MD,‡ Atsuki Kobayashi, MD,† Yorito Anamizu, MD,§ Junji Kishimoto, MA,¶ Kazuto Hoshi, MD,* Katsushi Takeshita, MD,* and Kozo Nakamura, MD*

Study Design. Randomized controlled trial.

Objective. To examine the effect of limaprost, an oral prostaglandin (PG) E1 derivative, on health-related quality of life (HRQOL) in patients with symptomatic lumbar spinal stenosis (LSS), compared to etodolac, a NSAID.

Summary of Background Data. Limaprost, an oral PGE1 derivative, was developed in Japan to treat numerous ischemic symptoms of thromboangiitis obliterans (TAO) and LSS. Previous studies have demonstrated the effectiveness of limaprost in the symptoms in patients with LSS. However, the evidence for effect on patient-reported outcomes, such as patient's HRQOL or satisfaction, is limited.

Methods. This study was conducted at 4 study sites in Japan. Briefly, inclusion criteria were: age between 50 and 85 years; presence of both neurogenic intermittent claudication (NIC) and cauda equina symptoms (at least presence of bilateral numbness in the lower limbs); and MRI-confirmed central stenosis with acquired degenerative LSS. Limaprost (15 μg/d) or etodolac (400 mg/d) was administered for 8 weeks. The primary outcome was Short Form (SF)-36, and the secondary outcomes were the verbal rating scale of low back pain and leg numbness, walking distance, subjective improvement, and satisfaction.

Results. A total of 79 participants were randomized (limaprost:etodolac = 39:40). Thirteen participants withdrew from the study (limaprost:etodolac = 5:8) and 66 completed the study (limaprost:etodolac = 34:32). Comparisons showed that limaprost resulted in significantly greater improvements in the SF-36 subscales of physical functioning, role physical, bodily pain, vitality, and mental health. Limaprost was also significantly better than etodolac for leg numbness, NIC distance, and subjective improvement and satisfaction. In the subgroup analysis stratified by symptom severity, limaprost seemed more effective for milder symptoms. No serious adverse effects were reported in either treatment group.

Conclusion. In this study, limaprost was found to be efficacious on most outcome measures, such as HRQOL, symptoms and subjective satisfaction, in LSS patents with cauda equina symptoms.

Key words: lumbar spinal stenosis, limaprost, neurogenic intermittent claudication. **Spine 2009;34:115–120**

Lumbar spinal stenosis (LSS) is a neurologic syndrome caused by vertebral degeneration.[1,2] Patients usually present with low back pain, leg pain, and leg numbness. These symptoms are exacerbated by lumbar extension but relieved by flexion. The cardinal symptom of LSS is neurogenic intermittent claudication (NIC).[3] Symptoms associated with LSS generally decrease the quality of life of patients, which may cause them to seek treatment. Initial treatment of LSS is not surgical intervention but conservative management because rapid neurologic progression and cauda equina syndrome are rarely seen[4] and also because patients are often elderly. Drug therapy is usually used in patients with mild to moderate symptoms. As far as pharmacotherapy is concerned, nonsteroidal anti-inflammatory drugs (NSAIDs) have primarily been administered.[4,5]

Although the pathogenesis of LSS symptoms remains controversial, mechanical compression of the cauda equina and nerve roots by the degenerative lumbar spine or the related soft tissues including thickened ligamentum flavum disturb vascular circulation of neural elements in the spinal canal. In other words, a state of relative ischemia in nerve tissues is a potential mechanism causing NIC.[6–17]

Prostaglandin (PG) E1 is a vasodilator that increases blood flow and inhibits platelet aggregation. Intravenous PGE1 is primarily used for chronic peripheral arterial occlusive diseases (PAOD) and erectile dysfunction (ED) in the United States and Europe. Limaprost is an oral PGE1 derivative that was developed in Japan to treat ischemic symptoms of thromboangiitis obliterans (TAO) and LSS because of the well-known vasodilatory and antiplatelet properties. The efficacy of oral limaprost was evaluated in adult Japanese patients in 3 randomized, double-blind, 6-week trials.[18] One study included patients with TAO and 2 trials included patients with LSS.

Previous studies have demonstrated the effectiveness of limaprost in the symptoms of patients with LSS. However, the evidence of the effect on patient-based outcomes, such as patient's HRQOL or satisfaction, is limited. As well as symptomatic assessment, HRQOL

From the *Department of Orthopaedic Surgery, Faculty of Medicine, University of Tokyo, Tokyo, Japan; †Japanese Red Cross Medical Center, Tokyo, Japan; ‡Musashino Red Cross Hospital, Tokyo, Japan; §Tokyo Metropolitan Geriatric Hospital, Tokyo, Japan; and ¶The University of Kyushu, Fukuoka, Japan.

Acknowledgment date January 10 2008. First revision date: June 05, 2008. Second revision date: August 24, 2008. Acceptance date: August 25, 2008.

The device(s)/drug(s) that is/are the subject of this manuscript is/are not FDA-approved for this indication and is/are not commercially available in the United States.

No funds were received in support of this work. No benefits in any form have been or will be received from a commercial party related directly or indirectly to the subject of this manuscript.

Address correspondence and reprint request to Ko Matsudaira, MD, Department of Orthopaedic Surgery, Faculty of Medicine, University of Tokyo, 7-3-1 Hongo, Bunkyo-ku, Tokyo 113-0033, Japan; E-mail: kohart801@gmail.com

Copyright © Lippincott Williams & Wilkins. Unauthorized reproduction of this article is prohibited.

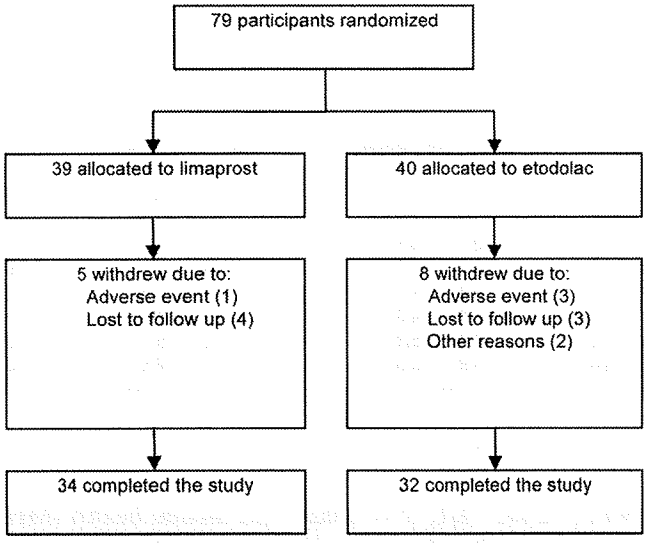

Figure 1. Flow chart showing flow of participants though the study.

assessment is also crucial to assess the treatment of a disabling chronic condition like LSS. The primary objective of this study was to examine the effect of limaprost on health-related quality of life (HRQOL), compared to etodolac,[19] a NSAID, which is commonly used in drug therapy for LSS.

■ Materials and Methods

This randomized, open-label, active-controlled trial was conducted at 4 study sites in Japan as follows: the University of Tokyo Hospital, Tokyo Metropolitan Geriatric Hospital, Japanese Red Cross Medical Center, and Musashino Red Cross Hospital. The study protocol was reviewed and approved by the ethics committees of all the study sites. All participants provided written informed consent before study procedures were initiated.

Patients who met the following eligibility criteria were enrolled in the study. Briefly, inclusion criteria were: age between 50 and 85 years; presence of both NIC and cauda equina symptoms (at least presence of bilateral numbness in the lower limbs); and MRI-confirmed central stenosis with acquired degenerative LSS.[20] Exclusion criteria were: presence of radicular leg pain only; positive straight leg raising (SLR) test with suspected lumbar disc herniation; presenting lower extremity peripheral arterial occlusive diseases PAOD (arteries of foot unpalpable and ankle brachial pressure index of <0.9); history of spinal surgery, myelopathy, peripheral neuropathy such as diabetic neuropathy of the leg; disorders potentially hindering gait besides LSS, *i.e.*, severe visual impairment, cerebral infarction, parkinsonism, rheumatoid arthritis, reduced cardiopulmonary function, or digestive, hematological, hepatic and/or renal disorders; or use of cardiac medication, *i.e.*, vasodilators or antiplatelet agents, or antidepressant medication.

Eligible patients were randomly allocated either to the limaprost or the etodolac group. Allocation to the groups was performed by the University Hospital Medical Information Network (UMIN), which was completely independent from the study sites, through a central web-based registration system. The minimization technique was used in random allocation to ensure balance on the following 4 factors: age (<75 years/≥75 years), gender, severity (mild/severe; definition of severe symptoms is the existence of perineal symptoms including urinary disturbance, and/or leg numbness while resting), and study site. Participants were randomly allocated to receive 15 μg of limaprost 3 times a day, or 400 mg of etodolac, NSAID, twice a day. Both treatments were administered for 8 weeks in an open-label fashion. Analgesics, anti-inflammatory agents, muscle relaxants, calcitonin, and methycobalamin were prohibited. If any of these drugs had been used, a 2-week washout period was established. During the study period, injection therapy, such as root block, epidural block, trigger point injection, physical therapy, or the use of a flexion brace, was also not allowed.

The primary efficacy outcome was SF-36[21,22] version 2 score, ranging from 0 to 100. The secondary efficacy outcomes were the verbal rating scales (rating score of 6: none, slight, mild, moderate, strong, and severe) of low back pain, leg pain and leg numbness, walking distance (rating score of 5: ≥1000 m, ≥500 m, ≥100 m, <100 m, and a few gait), and subjective improvement (rating score of 4: improved, slightly improved, unchanged, and became worse) and satisfaction (4 ranting score: satisfied, slightly satisfied, slightly dissatisfied and dissatisfied). These outcomes were measured at baseline and then at week 8 after administration. All reported or observed adverse events were recorded at each visit.

Statistical Analysis

Assessments were conducted of all efficacy outcomes for participants who received at least 1 dose of study drug and had had a baseline assessment and a final assessment. Between-group differences in mean changes from baseline on the SF-36 subscales were analyzed by the independent samples *t* test unless its assumptions were violated, defined in the protocol as the primary efficacy analysis. Secondary efficacy outcomes, which all were ordered categorical response variables, were analyzed by the Cochran-Mantel-Haenszel statistics to test for association between study drug and response. Baseline adjustments were made for all the outcomes except patient-reported improvement and satisfaction. In addition, both efficacy outcomes were also analyzed in relation to the degree of symptom severity. Safety assessments were based on all participants who received at least 1 dose of study drug. Adverse events were summarized descriptively. All statistical tests were 2-tailed, and the significance level was fixed at 0.05 throughout. All computations were performed using SAS version 9.1 and JMP 7.0.

Table 1. Baseline Characteristics of the Participants

Characteristic	Limaprost Group (n = 34)	Etodolac Group (n = 32)
Age (yrs)		
≥75	12	12
<75	22	20
Mean ± SD	69.6 ± 9.0	72.2 ± 8.2
Sex		
Male:Female	20:14	22:10
Symptom severity		
Mild	17	16
Severe	17	16
Study center		
University of Tokyo Hospital	24	22
Japanese Red Cross Medical Center	5	4
Musashino Red Cross Hospital	2	2
Tokyo Metropolitan Geriatric Hospital	3	4

Values are n unless otherwise stated.

Copyright © Lippincott Williams & Wilkins. Unauthorized reproduction of this article is prohibited.

Table 2. Primary Efficacy Outcomes: SF-36 Subscale Scores

SF-36 Subscales	Limaprost Group (n = 34) Baseline	Limaprost Group (n = 34) Wk 8	Etodolac Group (n = 32) Baseline	Etodolac Group (n = 32) Wk 8	Limaprost Group Change From Baseline	Etodolac Group Change From Baseline	P*
Physical functioning	56.9 ± 20.0	67.9 ± 19.1	55.7 ± 21.1	57.3 ± 22.4	11.0 ± 14.6	1.6 ± 14.9	0.01
Role physical	61.8 ± 26.6	73.0 ± 24.5	62.9 ± 24.3	60.4 ± 32.7	11.2 ± 22.0	−2.5 ± 27.0	0.03
Bodily pain	42.3 ± 15.0	56.0 ± 18.7	47.0 ± 18.3	45.2 ± 18.3	13.7 ± 20.6	−1.8 ± 12.1	<0.01
General health	53.5 ± 17.5	57.8 ± 17.5	58.7 ± 17.7	56.4 ± 17.1	4.3 ± 11.2	−2.3 ± 18.1	0.08
Vitality	57.5 ± 23.1	64.7 ± 19.2	64.8 ± 23.4	60.7 ± 24.2	7.2 ± 19.9	−4.1 ± 17.4	0.02
Social functioning	70.2 ± 25.9	79.8 ± 25.7	69.1 ± 22.9	70.7 ± 23.2	9.6 ± 24.0	1.6 ± 22.6	0.17
Role emotional	68.1 ± 27.0	75.7 ± 20.9	65.6 ± 22.4	63.0 ± 31.0	7.6 ± 19.3	−2.6 ± 25.7	0.07
Mental health	66.3 ± 20.6	73.7 ± 17.2	71.1 ± 23.3	65.8 ± 23.0	6.9 ± 16.0	−5.3 ± 16.6	<0.01

Values are mean ± SD.
*The independent samples *t* test.

■ Results

A total of 79 participants were enrolled and randomized to receive study treatment between June 2002 and January 2005. Of these, 39 participants received limaprost, and 40 received etodolac (Figure 1). Thirteen participants withdrew during the study: 5 from the limaprost group (1 adverse event and 4 lost to follow-up) and 8 participants from the etodolac group (3 adverse events, 3 lost to follow-up and 2 for another reason). Thus, a total of 34 participants in the limaprost group and 32 in the etodolac group were assessed after the completion of the study. Baseline characteristics were similar between treatment groups (Table 1).

In the primary efficacy assessment, compared to the etodolac group, the limaprost group had a significantly greater improvement in the SF-36 subscales of physical functioning (PF) (mean change of limaprost *vs.* etodolac: 11.0 *vs.* 1.6, $P = 0.01$), role physical (RP) (11.2 *vs.* −2.5, $P = 0.03$), bodily pain (BP) (13.7 *vs.* −1.8, $P < 0.01$) for the physical health component summary and vitality (VT) (7.2 *vs.* −4.1, $P = 0.02$), and mental health (MH) (6.9 *vs.* −5.3, $P < 0.01$) for the mental health component summary (Table 2). Improvement trends for other subscales, such as general health (GH) for the mental health component summary and social functioning (SF) and role emotional (RE) for the mental health component summary, were also impressive in limaprost, but they did not reach statistical significance (mean change of limaprost *vs.* etodolac, *P* value: 4.3 *vs.* −2.3, $P = 0.08$; 9.6 *vs.* 1.6, $P = 0.17$; and 6.9 *vs.* −5.3, $P = 0.07$, respectively). In the additional analysis stratified by symptom severity, the subscales that demonstrated significantly higher scores in limaprost were: PF, BP, VT, and MH among participants with mild symptoms ($P = 0.04$, $P < 0.01$, $P = 0.03$ and $P < 0.01$, respectively); and BP among those with severe symptoms ($P = 0.02$) (Table 3). Overall, limaprost showed better results in the mild group, compared to the severe group. In addition, the results of the stratified analysis indicated the same directional effects as the overall results, favoring limaprost instead of

Table 3. Primary Efficacy Outcomes: SF-36 Subscale Scores by Symptom Severity

SF-36 Subscales	Severity	Limaprost Group (n = 34)* Baseline	Limaprost Group (n = 34)* Wk 8	Etodolac Group (n = 32)* Baseline	Etodolac Group (n = 32)* Wk 8	Limaprost Group Change From Baseline	Etodolac Group Change From Baseline	P†
Physical functioning	Mild	61.8 ± 18.1	77.5 ± 12.9	61.4 ± 19.3	64.4 ± 22.7	15.7 ± 17.6	3.0 ± 15.4	0.04
	Severe	52.1 ± 21.1	58.3 ± 19.7	50.0 ± 21.8	50.2 ± 20.3	6.3 ± 9.0	0.2 ± 14.8	0.16
Role physical	Mild	60.7 ± 31.2	74.6 ± 25.0	66.0 ± 25.2	69.5 ± 26.6	14.0 ± 19.3	3.5 ± 19.4	0.13
	Severe	62.9 ± 21.9	71.3 ± 21.5	59.8 ± 23.8	51.2 ± 36.3	8.5 ± 24.6	−8.6 ± 32.4	0.10
Bodily pain	Mild	43.5 ± 17.2	62.2 ± 20.3	49.6 ± 19.1	48.4 ± 15.7	18.6 ± 24.9	−1.2 ± 13.0	<0.01
	Severe	41.0 ± 12.9	49.8 ± 15.0	44.4 ± 17.8	41.9 ± 20.5	8.8 ± 14.3	−2.4 ± 11.6	0.02
General health	Mild	54.1 ± 19.0	59.9 ± 18.5	64.4 ± 16.8	62.2 ± 16.6	5.8 ± 11.3	−2.2 ± 17.6	0.13
	Severe	52.8 ± 16.5	55.6 ± 16.8	53.1 ± 17.2	50.6 ± 16.0	2.8 ± 11.2	−2.5 ± 19.3	0.34
Vitality	Mild	61.8 ± 22.0	69.1 ± 18.2	74.2 ± 16.0	69.1 ± 17.1	7.4 ± 19.2	−5.1 ± 11.7	0.03
	Severe	53.3 ± 24.1	60.3 ± 19.8	55.5 ± 26.2	52.3 ± 27.8	7.0 ± 21.2	−3.1 ± 22.1	0.19
Social functioning	Mild	71.3 ± 27.9	80.1 ± 28.7	71.1 ± 22.7	71.1 ± 22.7	8.8 ± 16.4	0.0 ± 25.0	0.24
	Severe	69.1 ± 24.7	79.4 ± 23.4	67.2 ± 23.7	70.3 ± 24.5	10.3 ± 30.4	3.1 ± 20.7	0.44
Role emotional	Mild	70.1 ± 30.5	77.0 ± 22.9	71.9 ± 19.0	69.8 ± 29.2	6.9 ± 13.6	−2.1 ± 22.5	0.17
	Severe	66.2 ± 23.8	74.5 ± 19.2	59.4 ± 24.3	56.3 ± 32.3	8.3 ± 24.1	−3.1 ± 29.3	0.23
Mental health	Mild	66.8 ± 21.9	75.6 ± 16.8	80.9 ± 14.5	74.7 ± 15.0	8.8 ± 15.9	−6.3 ± 14.0	<0.01
	Severe	65.9 ± 19.8	70.9 ± 17.9	61.3 ± 26.5	56.9 ± 26.4	5.0 ± 16.4	−4.4 ± 19.3	0.14

Values are mean ± SD.
*For limaprost, mild:severe = 17:17; and for etodolac, mild:severe = 16:16.
†The independent samples *t* test.

Copyright © Lippincott Williams & Wilkins. Unauthorized reproduction of this article is prohibited.

Table 4. Secondary Efficacy Outcomes: Low Back Pain, Leg Pain, and Leg Numbness

		Limaprost Group (n = 34)		Etodolac Group (n = 32)		
Outcome	Severity	Baseline	Wk 8	Baseline	Wk 8	P*
Low back pain	None	6	7	4	7	0.77
	Slight	1	8	5	5	
	Mild	8	9	6	6	
	Moderate	16	7	11	9	
	Strong	3	2	4	3	
	Severe	0	1	2	2	
Leg pain	None	2	2	4	2	0.08
	Slight	2	4	0	4	
	Mild	1	15	5	6	
	Moderate	19	8	13	11	
	Strong	9	4	7	7	
	Severe	1	1	3	2	
Leg numbness	None	0	3	0	0	<0.01
	Slight	3	8	0	1	
	Mild	5	10	4	2	
	Moderate	15	9	14	17	
	Strong	7	3	13	9	
	Severe	4	1	1	3	

Values are n.
*The Cochran-Mantel-Haenszel test, adjusting for baseline value.

etodolac; however, the magnitudes of the effects were changed, and some of the effects failed to reach statistical significance (Table 3).

Secondary efficacy outcomes significantly favoring limaprost over etodolac included leg numbness ($P < 0.01$) (Table 4), walking distance ($P < 0.01$) (Table 5), and subjective improvement and satisfaction ($P < 0.01$ for both) (Table 6). The secondary outcomes of low back pain and leg pain tended to be better for the limaprost group without achieving statistical significance ($P = 0.77$ and $P = 0.08$, respectively) (Table 4). The stratified analysis did not alter the overall results. In addition, the secondary outcomes were stratified by symptom severity and analyzed in the same manner. The stratified analysis did not alter the overall results, with the exception of walking distance not being statistically significant in the mild group (limaprost *vs.* etodolac: for low back pain, $P = 0.26$ in mild and $P = 0.52$ in severe; leg pain, $P = 0.12$ mild and $P = 0.78$ severe; leg numbness, $P < 0.01$ mild and $P < 0.01$ severe; walking distance, $P = 0.03$ mild and $P = 0.07$ severe; subjective improvement; $P < 0.01$ mild and $P < 0.01$ severe; and subjective satisfaction, $P < 0.01$ mild and $P = 0.01$ severe).

Table 5. Secondary Efficacy Outcomes: Neurogenic Intermittent Claudication (NIC) Distance

	Limaprost Group (n = 34)		Etodolac Group (n = 32)		
Distance	Baseline	Wk 8	Baseline	Wk 8	P*
≥1000m	2	9	5	4	<0.01
≥500m	12	9	8	7	
≥100m	11	10	11	9	
<100m	8	6	8	12	
A few gait	1	0	0	0	

*The Cochran-Mantel-Haenszel test, adjusting for baseline value.

During the study, 3 participants in the limaprost group and 3 in the etodolac group reported a minor adverse event. In the limaprost group, 1 participant experienced hot flashes/flushing and anorexia a few days after administration, leading to withdrawal from the study, and 2 complained of stomach discomfort (digestive tract symptoms) at the start of administration and 4 weeks after administration, respectively. However, both of them completed the study because the reported event disappeared a few days later. In the etodolac group, 2 participants reported gastric pain and 1 diarrhea and all of them withdrew from the study at week 2, week 4, and week 1 after administration, respectively. No serious adverse events were reported in either treatment group.

■ Discussion

The results of this study suggested that limaprost might be more efficacious than etodolac in LSS patients with cauda equina symptoms. In the comparison of SF-36 subscales between the 2 drug groups, limaprost proved significantly better than etodolac in improving both the physical (PF, RP, and BP) and mental health (VT and MH) component summaries. In the secondary efficacy assessment, leg numbness, walking distance, and patient-reported improvement and satisfaction were significantly improved in the limaprost group over the etodolac group. In the subgroup of patients with milder symptoms, not consisting of perineal symptoms including urinary disturbance and/or leg numbness while resting, limaprost seemed more effective. Increasing physical activities resulting from symptom improvement promote sequential improvements in mental and emotional factors. This might be part of the reason for improvements of the mental component summary, such as VT and MH.

In Japan, limaprost was approved in 1988 with an indication for the "improvement of various ischemic symptoms, such as ulcer, pain, and feeling of coldness associated with TAO." It was also approved in 2001 with an indication for "the improvement of subjective symptoms (pain and numbness of lower legs) and gait ability associated with acquired LSS." In a phase III trial in LSS patients, limaprost was considered by investigators to provide an overall improvement from baseline to study end and to improve an overall drug usefulness.[18] Assessment of overall improvement considered symptoms (*e.g.*, leg pain or numbness, walking distance), whereas overall usefulness also considered safety issues. Our study provides significant improvements in leg numbness and walking distance, which was consistent with the above phase III trial. However, there was no significant improvement in low back pain and leg pain. According to previous studies, including postmarketing studies, limaprost was safely administered and well tolerated. In the postmarketing surveillance where 1930 patients with LSS took limaprost for a mean duration of

Copyright © Lippincott Williams & Wilkins. Unauthorized reproduction of this article is prohibited.

Table 6. Secondary Efficacy Outcomes: Patient's Subjective Improvement and Satisfaction

Outcome	Subjective Rating	Limaprost Group (n = 34) n (%)	Etodolac Group (n = 32) n (%)	P*
Patient's subjective Improvement	Improved	11 (32.4)	0 (0)	<0.01
	Slightly improved	14 (41.2)	6 (18.8)	
	Unchanged	8 (23.5)	19 (59.4)	
	Became worse	1 (2.9)	7 (21.9)	
Patient's subjective Satisfaction	Satisfied	14 (41.2)	1 (3.1)	<0.01
	Slightly satisfied	17 (50.0)	13 (40.6)	
	Slightly dissatisfied	2 (5.9)	16 (50.0)	
	Dissatisfied	1 (2.9)	2 (6.3)	

Values are n (%).
*The Cochran-Mantel-Haenszel test.

approximately 4 months, the overall incidence of treatment-related adverse effects occurred in 5.2% of patients. One serious adverse event (bleeding duodenal ulcer) was reported (<0.001% in total). The common adverse effects included gastrointestinal (GI)-related effects and hot flushes/flushing. These effects were usually not serious. The safety findings of our study were in general agreement with the findings in other studies.

Elderly people sometimes have comorbidities, and patients, as well as physicians, seek effective conservative treatment. However, nonoperative approaches have been limited to NSAIDs and physical treatment, and the actual effectiveness of these has not been sufficiently studied. NSAIDs are usually administered for pain control,[4,5] but no RCTs have been conducted to assess the efficacy of NSAIDs. Although several RCTs assessing the efficiency of calcitonin have been performed since Porter and Miller's report,[23] sufficient evidence to support the efficacy of this drug has not been well established because contradictory findings were reported.[24–26] Recently, Yaksi *et al*[27] suggested that adding gabapentin to conventional therapy, such as physical therapy, brace therapy, and NSAIDs, may improve walking disturbance and pain. However, they concluded that the further evaluation for gabapentin was necessary because it was administered as an additional therapy. Thus, the investigations to assess pharmacotherapeutic options for LSS are still insufficient.

It has been reported that limaprost improved walking distance and blood flow of cauda equina tissue in a rat model with compressed cauda equina.[28] No such effects were observed with loxoprofen sodium (NSAID), ticlopidine (an antiplatelet), nifedipine (a vasodilator), or cilostazol (an antiplatelet and vasodilator) in the same model.[29,30] These findings may support limaprost's expected effectiveness for NIC by increasing blood flow in the cauda equina.

Several limitations of this study should be considered. First, owing to the absence of a placebo group, the placebo effect was not eliminated, which may have weakened the results of this study. Second, because the duration of treatment was 8 weeks, the results may not be generalizable to longer treatment periods. Third, the sample size may have been insufficient for a rigorous statistical analysis to detect true difference between the groups. Finally, the results may generalize to patients only if they are similar in patient characteristics of this study. The fact that LSS patients generally have various comorbidities may limit the generalizability of the study results.

■ Conclusion

In this randomized controlled trial, limaprost was found to be efficacious on most outcome measures, such as HRQOL, symptoms, and subjective satisfaction, in LSS patents with cauda equina symptoms. Limaprost also seemed more effective for patients with milder symptoms, compared to those with more severe symptoms. Together with previous findings, limaprost can be considered to a likely candidate for drug therapy in LSS with cauda equine symptoms. Further studies with placebo-controls, longer treatment periods, larger sample sizes, and a variety of study populations are warranted to learn more about clinical benefits are recommended.

■ Key Points

- In this randomized controlled trial, the efficacy of limaprost, an oral PGE1 derivative, on the HRQOL and the clinical symptoms in patients with cauda equina symptoms of LSS, was examined, compared to etodolac, a NSAID. Thirty-two etodolac patients and 34 limaprost patients were analyzed.
- In terms of differences between baseline and 8-week SF-36 scores, the limaprost group showed significant improvement not only in PF, RP, BP, VT, and MH but also in leg numbness and walking distance, compared to the etodolac group. In the subgroup analysis stratified by symptom severity, limaprost seemed more effective for milder symptoms. No serious adverse events were reported in either treatment group.
- Limaprost can be considered to a likely candidate for drug therapy in LSS with cauda equine symptoms.

Copyright © Lippincott Williams & Wilkins. Unauthorized reproduction of this article is prohibited.

References

1. Berthelot JM, Bertrand VA, Rodet D, et al. Lumbar spinal stenosis: a review. *Rev Rhum Engl Ed* 1997;64:315–25.
2. Bolander NF, Schonstrom NSR, Spengler DM. Role of computed tomography and myelography in the diagnosis of central spinal stenosis. *J Bone Joint Surg Am* 1985;67A:240–6.
3. Takahashi K, Miyazaki T, Takino T, et al. Epidural pressure measurements; relationship between pressure and posture in patients with lumbar spinal stenosis. *Spine* 1995;20:650–3.
4. Yuan PS, Booth RE Jr, Albert TJ. Nonsurgical and surgical management of lumbar spinal stenosis. *Instr Course Lect* 2005;54:303–12.
5. Hilibrand AS, Rand N. Degenerative lumbar stenosis. *J Am Acad Orthop Surg* 1999;7:239–49.
6. Blau JN, Louge V. Intermittent claudication of cauda equine. *Lancet* 1961; 1:1081–6.
7. Cavanaugh GJ, Svein J, Holman CB, et al. 'Pseudoclaudication' syndrome produced by compression of cauda equina. *JAMA* 1968;206:2477–81.
8. Parke WW, Watanabe R. The intrinsic vasculature of the lumbosacral spine nerve roots. *Spine* 1985;6:508–61.
9. Ooi Y, Mita F, Satoh Y. Myeloscopic study on lumbar spinal stenosis with special reference to intermittent claudication. *Spine* 1990;15:544–9.
10. Delamarter RB, Bohlam HH, Dodge LD, et al. Experimental lumbar spinal stenosis; analysis of the cortical evoked potentials, microvasculature and histopathology. *J Bone Joint Surg Am* 1990;72-A:110–20.
11. Olmarker K, Holm S, Rydevik B. Experimental nerve root compression. A model of acute graded compression of the porcine cauda equine and analysis of neural and vascular anatomy. *Spine* 1991;16:61–9.
12. Takahashi K, Olmarker K, Holm S, et al. Double level cauda equine compression: an experimental study with continuous monitoring of intraneural blood flow in the porcine cauda equine. *J Orthop Res* 1993;11:104–9.
13. Konno S, Sato K, Yabuki S, et al. A model for acute, chronic and delayed graded compression of the dog cauda equine; presentation of the gross, microscopic, and vascular in pressure transmission of the compression model. *Spine* 1995;20:2758–64.
14. Konno S, Olmarker K, Byröd G, et al. Intermittent cauda equine compression; an experimental study on the procine cauda equine with analysis of nerve impulse conduction properties. *Spine* 1995;20:1223–6.
15. Sato K, Yabuki S, Konno S, et al. A model for acute, chronic, and delayed graded compression of the dog cauda equine; neurophysiology and histologic change induced by acute, graded compression. *Spine* 1995;20: 2386–91.
16. Kikuchi S, Konno S, Kayama S, et al. Increased resistance to acute compression injury in chronically compressed spinal root. *Spine* 1996;21:2544–50.
17. Kobayashi S, Yoshizawa H, Nakai S. Experimental study on dynamics of lumbosacral nerve root circulation. *Spine* 2000;25:298–305.
18. Harrison TS, Plosker GL. Limaprost. *Drugs* 2007;67:109–18.
19. Hatori M, Kokubun S. Clinical use of etodolac for treatment of lumbar disc herniation. *Curr Med Res Opin* 1999;15:193–201.
20. Arnoldi CC, Brodsky AE, Cauchoix J, et al. Lumbar spinal stenosis and nerve root entrapment: syndrome, definition, and classification. *Clin Orthop* 1976;115:4–5.
21. Fukuhara S, Bito S, Green J, et al. Translation, adaptation, and validation of the SF-36 health survey for use in Japan. *J Clin Epidemiol* 1998;51:1037–44.
22. Fukuhara S, Ware JE, Kosinski M, et al. Psychometric and clinical tests of validity of the Japanese SF-36 health survey. *J Clin Epidemiol* 1998;51: 1045–53.
23. Porter RW, Miller CG. Neurogenic claudication and root claudication treated with calcitonin: a double-blind trial. *Spine* 1988;13:1061–4.
24. Eskola A, Pohjolainen T, Alaranta H, et al. Calcitonin treatment in lumbar spinal stenosis: a randomized, placebo-controlled, double-blind, cross-over study with one-year follow-up. *Calcif Tissue Int* 1992;50:400–3.
25. Podichetty VK, Segal AM, Lieber M, et al. Effectiveness of salmon calcitonin nasal spray in the treatment of lumbar canal stenosis, a double-blind, randomized, placebo-controlled, parallel group trial. *Spine* 2004;29:2343–9.
26. Tafazal SI, Ng L, Sell P. Randomised placebo-controlled trial on the effectiveness of nasal salmon calcitonin in treatment of lumbar spinal stenosis. *Eur Spine J* 2007;16:207–12.
27. Yaksi A, Özgönenel L, Özgönenel B. The efficiency of gabapentin therapy in patients with lumbar spinal stenosis. *Spine* 2007;32:939–42.
28. Nakai K, Takenobu Y, Eguchi K, et al. Effects of OP-1206 α-CD on walking dysfunction in the rat neuropathic intermittent claudication model. *Anesth Analg* 2002;94:1534–41.
29. Nakai K, Takenobu Y, Takimizu H, et al. Effects of orally administered OP-1206 α-CD with loxoprofen-Na on walking dysfunction in the rat neuropathic intermittent claudication model. *Prostaglandins Leukot Essent Fatty Acids* 2003;69:269–73.
30. Nakai K, Takenobu Y, Takimizu H, et al. Effects of OP-1206 α-CD on walking dysfunction in the rat neuropathic intermittent claudication model: comparison with nifedipin, ticlopidine and cilostazol. *Prostaglandins Other Lipid Mediat* 2003;71:253–63.

Copyright © Lippincott Williams & Wilkins. Unauthorized reproduction of this article is prohibited.

IFN-γ receptor signaling mediates spinal microglia activation driving neuropathic pain

Makoto Tsuda[1], Takahiro Masuda[1], Junko Kitano, Hiroshi Shimoyama, Hidetoshi Tozaki-Saitoh, and Kazuhide Inoue[2]

Department of Molecular and System Pharmacology, Graduate School of Pharmaceutical Sciences, Kyushu University, 3-1-1 Maidashi, Higashi-ku, Fukuoka, Fukuoka 812-8582, Japan

Edited by David Julius, University of California, San Francisco, CA, and approved March 18, 2009 (received for review October 16, 2008)

Neuropathic pain, a highly debilitating pain condition that commonly occurs after nerve damage, is a reflection of the aberrant excitability of dorsal horn neurons. This pathologically altered neurotransmission requires a communication with spinal microglia activated by nerve injury. However, how normal resting microglia become activated remains unknown. Here we show that in naive animals spinal microglia express a receptor for the cytokine IFN-γ (IFN-γR) in a cell-type-specific manner and that stimulating this receptor converts microglia into activated cells and produces a long-lasting pain hypersensitivity evoked by innocuous stimuli (tactile allodynia, a hallmark symptom of neuropathic pain). Conversely, ablating IFN-γR severely impairs nerve injury-evoked microglia activation and tactile allodynia without affecting microglia in the contralateral dorsal horn or basal pain sensitivity. We also find that IFN-γ-stimulated spinal microglia show up-regulation of Lyn tyrosine kinase and purinergic $P2X_4$ receptor, crucial events for neuropathic pain, and genetic approaches provide evidence linking these events to IFN-γR-dependent microglial and behavioral alterations. These results suggest that IFN-γR is a key element in the molecular machinery through which resting spinal microglia transform into an activated state that drives neuropathic pain.

allodynia | cytokine | glia | Lyn tyrosine kinase | purinergic receptor

Neuropathic pain is a chronic pain condition that occurs after nerve damage, such as that induced by bone compression in cancer, diabetes, infection, autoimmune disease, or physical injury (1). One troublesome hallmark symptom of neuropathic pain is pain hypersensitivity to normally innocuous stimuli, a phenomenon known as "tactile allodynia," which is refractory to currently available treatments such as nonsteroidal anti-inflammatories and opioids (2, 3). Accumulating evidence from diverse animal models of neuropathic pain suggests that neuropathic pain might involve aberrant excitability of the nervous system, notably at the levels of the primary sensory ganglia and the dorsal horn of the spinal cord, resulting from multiple functional and anatomical alterations following peripheral nerve injury (3, 4). Although it long was thought that these alterations occur mainly in neurons, emerging lines of evidence show that they also occur in spinal microglia, a group of immune cells (5–9). After injury to peripheral nerves, microglia in the normal state (traditionally called "resting" microglia) in the spinal dorsal horn are converted to an activated state through a series of cellular and molecular changes. Activated spinal microglia show hypertrophied soma, thickened and retracted processes, and increased proliferation activity (6, 9, 10). Furthermore, these microglia induce or enhance expression of various genes including neurotransmitter receptors (11) (e.g., $P2X_4R$, a subtype of ATP-gated cation channels (12)) and intracellular signaling kinases (e.g., mitogen-activated protein kinases (13–16) and Lyn tyrosine kinase (17)). By responding to extracellular stimuli such as ATP, the activated microglia evoke various cellular responses such as production and release of bioactive factors, including cytokines and neurotrophic factors (18, 19). Importantly, pharmacological, molecular, and genetic manipulations of the function or expression of these microglial molecules substantially influence nerve injury-induced pain behaviors (12–16, 20–22) and the hyperexcitability of the dorsal horn pain pathway (23, 24). Therefore, spinal microglia activated after nerve injury critically contribute to the pathologically enhanced pain processing in the dorsal horn that underlies neuropathic pain (5–9). Understanding how resting spinal microglia are transformed into activated cells after nerve injury may be an important step in unraveling the pathogenesis of neuropathic pain, but the mechanism remains unclear.

In the present study, we investigated this issue, focusing on the proinflammatory cytokine IFN-γ. IFN-γ is among the biologically active signaling molecules that have been reported to activate primary cultured microglial cells (25). A recent study has indicated that IFN-γ levels are increased in the spinal cord after nerve injury (20), leading to speculation that IFN-γ has a role in neuropathic pain. However, there is no direct evidence indicating that IFN-γ signaling contributes to microglia activation in the dorsal horn and tactile allodynia under neuropathic pain conditions. Here, we report that the receptor for IFN-γ (IFN-γR), which is constitutively expressed in normal resting microglia in the dorsal horn, is a key component in the molecular machinery through which peripheral nerve injury converts spinal microglia from the resting state to the activated state that underlies the pathogenesis of neuropathic pain.

Results

Stimulating IFN-γRs in Spinal Microglia Under Normal Conditions Induces Activation of Microglia and Long-Lasting Allodynia. We first investigated expression of IFN-γRs by in situ hybridization for IFN-γR mRNA on sections of the fifth lumbar (L5) dorsal spinal cord of naive rats. Signals for IFN-γR mRNA were detected readily in the dorsal horn (Fig. 1*A*, intense violet dots indicated by arrowheads); these signals were not observed in sections hybridized with a corresponding sense probe (Fig. 1*A*). Similar results were obtained with another set of cRNA probes for IFN-γR (data not shown). To identify the type of cells expressing IFN-γRs, we performed in situ hybridization combined with immunohistochemistry for ionized calcium-binding adapter molecule-1 (Iba1), a marker of microglia, and showed that the IFN-γR mRNA signals were restricted to cells labeled with Iba1 (arrowheads in Fig. 1*B*). In addition, IFN-γR protein also was detected in homogenates from the spinal cord of naive rats and microglial cells in culture in Western blot analysis (data not shown). To determine whether IFN-γRs are expressed as functional receptors in spinal microglia, we spinally administered recombinant IFN-γ to naive rats and immunohistochemically

Author contributions: M.T. and K.I. designed research; M.T., T.M., J.K., H.S., and H.T.-S. performed research; M.T., T.M., H.T.-S., and K.I. analyzed data; and M.T., T.M., and K.I. wrote the paper.

The authors declare no conflict of interest.

This article is a PNAS Direct Submission.

[1]M.T. and T.M. contributed equally to this work.

[2]To whom correspondence should be addressed. E-mail: inoue@phar.kyushu-u.ac.jp.

This article contains supporting information online at www.pnas.org/cgi/content/full/0810420106/DCSupplemental.

www.pnas.org/cgi/doi/10.1073/pnas.0810420106

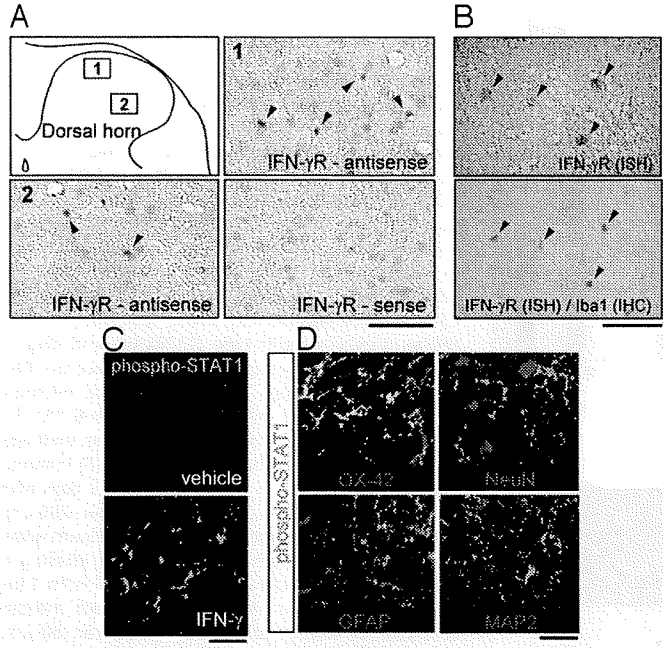

Fig. 1. IFN-γRs in the spinal cord are expressed in microglia under normal conditions. (*A*) In situ hybridization analysis of the IFN-γ receptor (IFN-γR) mRNA in the dorsal horns of normal rats (arrowheads indicate IFNγR mRNA signals.) (Scale bar, 80 μm.) (*B*) IFN-γR mRNA signals overlapped with immunoreactivity for Iba1 (arrowheads). IHC, immunohistochemistry; ISH, in situ hybridization. (Scale bar, 80 μm.) (*C*) Phospho-STAT1 immunofluorescence 15 min after IFN-γ injection. (Scale bar, 20 μm.) (*D*) Double immunofluorescence labeling for phospho-STAT1 (green) and cell-type markers (OX-42, a marker of microglia; GFAP, a marker of astrocytes; MAP2 and NeuN, markers of neurons). (Scale bar, 20 μm.)

examined the level of activated signal transducer and activator of transcription 1 (phospho-STAT1), a molecule downstream of IFN-γR (26). At 15 min after intrathecal IFN-γ administration (1,000 U), immunofluorescence of phospho-STAT1 was increased in the dorsal horn (Fig. 1*C*). Consistent with microglia-restricted localization of IFN-γR, STAT1 phosphorylation evoked by IFN-γ also occurred specifically in cells that were double-labeled with OX-42, a microglial marker, but not in cells labeled with glial fibrillary acidic protein (GFAP; an astrocyte marker) or with the neuronal markers microtubule-associated protein 2 (MAP2) or neuronal nuclei (NeuN) (Fig. 1*D*). STAT1 phosphorylation also was induced in cultured spinal microglial cells stimulated directly with IFN-γ (data not shown). These findings suggest that under normal conditions IFN-γRs are expressed as functional receptors in resting microglia in the dorsal horn.

To examine the in vivo responses evoked by IFN-γ, we spinally administered IFN-γ to naive rats and subsequently used a behavioral assay for tactile allodynia. We found that a single intrathecal administration of IFN-γ (1,000 U) produced marked and long-lasting tactile allodynia: the paw withdrawal threshold (PWT) to mechanical stimulation applied to the hindpaw progressively decreased over the first 2 days, peaking between days 2 and 3 ($P < 0.01$), and the decreased PWT persisted for at least 10 days after the administration ($P < 0.05$; Fig. 2*A*). The IFN-γ-induced allodynia was dose dependent (10 U: $P < 0.05$; 100 and 1,000 U: $P < 0.01$ on day 3; Fig. 2*B*). Although a similar allodynic behavior was produced in wild-type C57BL/6J mice injected intrathecally with IFN-γ (10 U, $P < 0.01$; Fig. 2*C*), IFN-γR-deficient (*ifngr*$^{-/-}$) mice failed to produce this response. Interestingly, we found that *ifngr*$^{-/-}$ mice that had been intrathecally infused with primary cultured microglia taken from wild-type C57BL/6J mice showed a decrease in the PWT after IFN-γ administration, but there was no change in threshold in *ifngr*$^{-/-}$ mice infused with *ifngr*$^{-/-}$ microglia (Fig. 2*D*). This finding suggests that IFNγ-induced allodynia impaired in *ifngr*$^{-/-}$ mice is rescued by infusing microglia expressing IFN-γR. In addition, the PWT was not affected by infusion of microglia from either wild-type C57BL/6J or *ifngr*$^{-/-}$ mice alone (data not shown). These results indicate that stimulating IFN-γRs in spinal microglia produces persistent tactile allodynia in otherwise naive animals.

These results prompted us to investigate the status of microglia in the dorsal horn after IFN-γR stimulation, and we performed immunohistochemical analyses on sections of L5 dorsal spinal cord. On day 3 after IFN-γ administration, microglial cells in the dorsal horn had enhanced Iba1 labeling, hypertrophic cell bodies, and thickened and shortened processes (Fig. 2*E*). By contrast, immunofluorescence of ED-1 (a macrophage marker) was not enhanced by IFN-γ, and neither the morphology nor the number of ED-1$^+$ cells was changed (SI Text and Fig. S1). In addition, only a very few circulating ED-1$^+$ macrophages were labeled by intravenously injected PKH26-PCL (Fig. S2), an inert fluorescent dye that selectively labels cells with phagocytic capabilities (27), suggesting that intrathecal administration of IFN-γ does not cause macrophage infiltration. Next, to test whether IFN-γ-stimulated microglia undergo proliferation, we visualized proliferating cells by administering i.p. a single dose of BrdU, a marker of the S-phase of the cell cycle. Intrathecal administration of IFN-γ drastically increased the number of BrdU$^+$Iba1$^+$ cells in the dorsal horn on day 1 ($P < 0.001$; Fig. 2*F*). In addition, we observed a few BrdU$^+$Iba1$^-$ cells in the dorsal horn, the number of which was not altered by IFN-γ (vehicle: 3.0 ± 1.5 cells; IFN-γ: 4.7 ± 2.2 cells). The proliferation of spinal microglia is strongly supported by our further immunohistochemical analyses demonstrating that the number of OX-42$^+$ microglia positive for Ki-67, a nuclear protein expressed in all phases of the cell cycle except the resting phase, also was increased in the dorsal horn of rats to which IFN-γ was administered (Fig. S3*A*). In addition, there were very few Ki-67$^+$ED-1$^+$ cells in the dorsal horn (Fig. S3*A*). By counting microglial cells within the dorsal horn on day 3, we observed that the total number of Iba1$^+$ microglia increased in rats treated with IFN-γ compared with rats treated with vehicle ($P < 0.01$; Fig. 2*G*). IFN-γ did not increase the number of OX-42$^+$ P2Y$_{12}$R$^-$ cells in the dorsal horn, and almost all OX-42$^+$ cells are double-labeled with an antibody of P2Y$_{12}$ purinoceptor (P2Y$_{12}$R) (Fig. S4), a G protein-coupled receptor that is expressed in microglia but not in macrophages (29, 30). These changes in the morphology and number of microglia in rats treated with IFN-γ are consistent with immunohistochemical criteria for activated microglia in vivo (28) and are observed in the dorsal horn after nerve injury (6).

We next tested the effect of minocycline, which inhibits microglia activation in vivo (31), on IFN-γ-induced tactile allodynia. Minocycline (40 mg/kg) suppressed the decrease in the PWT at all time points of testing ($P < 0.001$; Fig. 2*H*) as well as the activation of microglia in the dorsal horn on day 3 after intrathecal administration of IFN-γ (Fig. 2*H*). Together, these findings indicate that stimulation of spinal IFN-γRs expressed selectively in microglia under normal conditions causes tactile allodynia by directly activating spinal microglia.

Lack of IFN-γR Impairs Activation of Microglia and Tactile Allodynia After Nerve Injury. Next, to investigate the role of IFN-γR in microglia activation and tactile allodynia in the dorsal horn under neuropathic pain conditions, we injured the L5 spinal nerve of wild-type C57BL/6J and *ifngr*$^{-/-}$ mice, an animal model of neuropathic pain. Consistent with our previous studies (17,

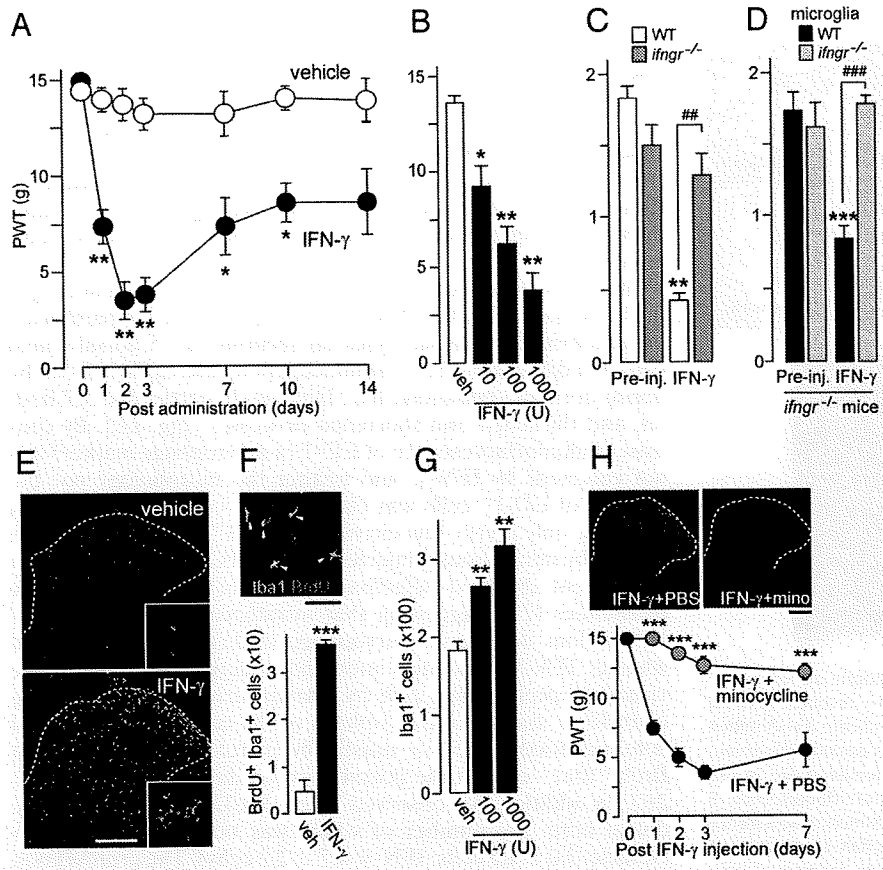

Fig. 2. Intrathecal delivery of IFN-γ to normal animals induces long-lasting tactile allodynia and activation of spinal microglia. (*A*) PWT after a single intrathecal administration of recombinant IFN-γ (1,000 U; $n = 6$) or vehicle (PBS; $n = 6$) to naive rats (*, $P < 0.05$; **, $P < 0.01$). (*B*) Dose-dependent tactile allodynia on day 3 ($n = 5$–6; *, $P < 0.05$; **, $P < 0.01$). (*C*) PWT in wild-type C57BL/6J ($n = 6$) and IFN-γR-deficient (*ifngr*$^{-/-}$) mice ($n = 6$) 3 days after IFN-γ (10 U) administration (**, $P < 0.01$ vs. before injection; ##, $P < 0.01$ vs. wild-type C57BL/6J mice injected with IFN-γ). (*D*) Effects of intrathecal infusion of wild-type (C57BL/6J) and *ifngr*$^{-/-}$ primary cultured microglia to *ifngr*$^{-/-}$ mice on IFN-γ (10 U)-induced change in PWT (wild-type microglia group, $n = 5$; *ifngr*$^{-/-}$ microglia group, $n = 6$; ***, $P < 0.0001$ vs. before injection; ###, $P < 0.0001$ vs. wild-type C57BL/6J microglia with IFN-γ injection). (*E*) Immunofluorescence of Iba1 in the dorsal horn 3 days after administration of IFN-γ (1,000 U). (Scale bar, 200 μm.) Insets are images at high magnification (45 μm wide). (*F*) (*Upper*) Double immunofluorescence labeling of Iba1 (green) with BrdU (red) in the dorsal horn 1 day after administration of IFN-γ (arrowheads indicate cells positive to Iba1 and BrdU). (Scale bar, 80 μm.) (*Lower*) The number of BrdU$^+$Iba1$^+$ cells in the dorsal horn of rats ($n = 3$; ***, $P < 0.001$). (*G*) The number of Iba1$^+$ microglia in the dorsal horn of vehicle- and IFN-γ-treated rats (**, $P < 0.01$). (*H*) Effect of minocycline (40 mg/kg, i.p.) on IFN-γ-induced microglia activation. Photographs show immunofluorescence of Iba1 on day 3 (scale bar, 200 μm) and tactile allodynia ($n = 5$; ***, $P < 0.001$ vs. IFN-γ/PBS group). Data are mean ± SEM (*A–D*, *F*, *G*, and *H*).

32), in wild-type C57BL/6J mice, a marked activation of microglia was observed on the ipsilateral side of the dorsal horn 14 days after nerve injury, as indicated by alterations in Iba1 immunofluorescence (Fig. 3*A*), morphology (Fig. 3*B*), and number ($P < 0.001$, Fig. 3*C*). However, these alterations in activated microglia were severely impaired in *ifngr*$^{-/-}$ mice with nerve injury, (Fig. 3 *A* and *B*), and the number of Iba1$^+$ cells was much lower than in wild-type C57BL/6J mice ($P < 0.001$; Fig. 3*C*). The number of microglia in the contralateral dorsal horn was similar in these 2 genotypes (Fig. 3*C*). Behaviorally, wild-type C57BL/6J mice showed a marked decrease in PWT after nerve injury (day 1: $P < 0.01$; days 3–14: $P < 0.001$; Fig. 3*D*). By contrast, the nerve injury-induced allodynic behavior was strikingly attenuated in *ifngr*$^{-/-}$ mice at all time points of testing (days 1 and 7: $P < 0.05$; days 3 and 5: $P < 0.01$; days 10 and 14: $P < 0.001$; Fig. 3*D*). The loss of IFN-γR did not change either basal mechanical sensitivity or the PWT of the contralateral hindpaw after nerve injury (Fig. 3*D*). Nor did IFN-γR deficiency affect motor behaviors in the rotarod test (time on rotarod for wild-type C57BL/6J: 55.4 ± 4.6 sec; for *ifngr*$^{-/-}$: 53.2 ± 6.8 sec). These findings indicate that IFN-γR-mediated signaling is required for switching spinal microglia to the activated phenotype in the spinal dorsal horn after nerve injury and for producing the subsequent tactile allodynia.

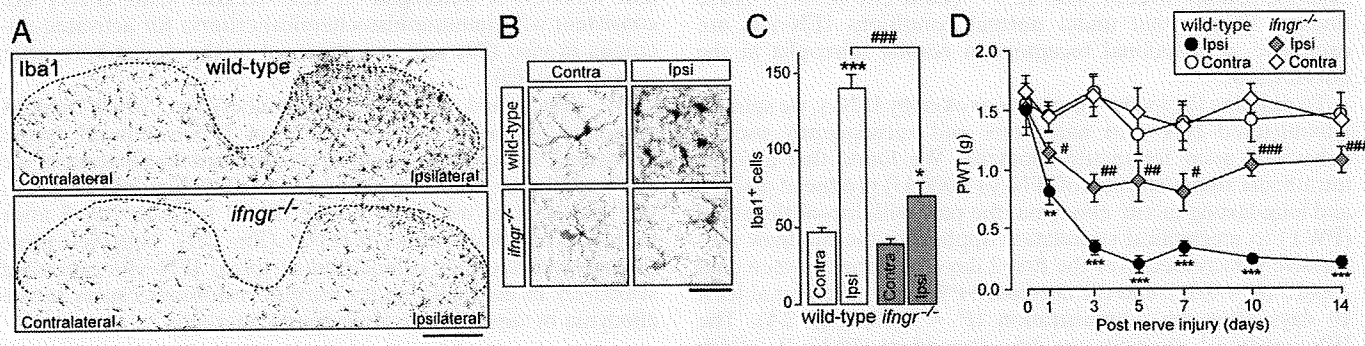

Fig. 3. Lack of IFN-γR impairs activation of microglia and tactile allodynia after nerve injury. (*A*) Photographs show immunofluorescence of Iba1 in the L5 dorsal spinal cord of wild-type C57BL/6J and *ifngr*$^{-/-}$ mice 14 days after nerve injury. (Scale bar, 150 μm.) (*B*) Morphological changes in the spinal microglia in the spinal dorsal horn of wild-type C57BL/6J or *ifngr*$^{-/-}$ mice. (Scale bar, 20 μm.) (*C*) The change in the number of Iba1-positive microglia cells in the dorsal horn of wild-type C57BL/6J ($n = 5$) and *ifngr*$^{-/-}$ ($n = 5$) mice 14 days after nerve injury (*, $P < 0.05$; ***, $P < 0.001$ vs. the contralateral side; ###, $P < 0.001$ vs. the ipsilateral side in wild-type C57BL/6J mice). (*D*) PWT of wild-type C57BL/6J ($n = 7$) and *ifngr*$^{-/-}$ mice ($n = 7$) before and after nerve injury (**, $P < 0.01$; ***, $P < 0.001$ vs. the contralateral side of wild-type C57BL/6J mice; #, $P < 0.05$; ##, $P < 0.01$; ###$P < 0.001$ vs. the ipsilateral side of wild-type C57BL/6J mice). Data are mean ± SEM (*C* and *D*).

Lyn Tyrosine Kinase Is a Critical Intermediary in the IFN-γR-Dependent Activation of Spinal Microglia. To elucidate the molecular mechanism by which IFN-γ activates spinal microglia, we examined the role of Src-family kinases (SFKs), which have been implicated in cellular responses including the proliferation of many types of cells (33). Among 5 major SFKs (Src, Fyn, Lck, Yes, and Lyn) known to be expressed in the CNS (34), expression of Lyn in spinal microglia, which is essential for tactile allodynia after nerve injury, is up-regulated and activated by nerve injury (17). In the spinal cord of animals administered IFN-γ intrathecally, expression of Lyn protein was increased 1 day after the administration ($P < 0.05$; Fig. 4*A*), and this increased expression was observed selectively in microglia labeled by Iba1 (Fig. 4*B*). When cultured microglial cells were treated with IFN-γ, the up-regulation of Lyn expression also was observed in a dose-dependent manner (Fig. 4*C*). We also found that immunofluorescence for the active form of SFKs, including Lyn, that were autophosphorylated in the kinase domain (phospho-SFK) increased exclusively in microglia labeled by OX-42 in the dorsal horn after intrathecal administration of IFN-γ (Fig. 4*D*), suggesting that Lyn kinase may become activated in spinal microglia stimulated by IFN-γ. To determine the in vivo role of Lyn kinase, we spinally administered IFN-γ to wild-type C57BL/6J and Lyn-knockout ($lyn^{-/-}$) mice. In contrast to the changes in the morphology (Fig. 4*E*) and number of microglia ($P < 0.01$; Fig. 4*F*) in the dorsal horn of wild-type C57BL/6J mice following IFN-γ administration, dorsal horn microglia lacking Lyn showed less activated morphology (Fig. 4*E*) and a smaller increase in number ($P < 0.05$; Fig. 4*F*). The loss of Lyn also blunted the decrease in PWT following intrathecal administration of IFN-γ ($P < 0.01$; Fig. 4*G*). Moreover, the nerve injury-induced increase in the number of microglial cells in the ipsilateral dorsal horn was lower in $lyn^{-/-}$ mice than in wild-type C57BL/6J mice ($P < 0.001$; Fig. 4*H*). These results indicate that Lyn tyrosine kinase is a critical intermediary in the activation of microglia caused by IFN-γ administration and nerve injury.

$P2X_4$ Receptors Up-Regulated in Microglia Are Required for IFN-γ-Induced Allodynia. Following nerve injury, activated spinal microglia up-regulate expression of $P2X_4$ receptors ($P2X_4Rs$), a principal subtype of ATP-gated ion channels crucial for neuropathic pain (12, 23). We therefore determined whether IFN-γR-induced allodynia involves $P2X_4Rs$. Applying IFN-γ directly to primary cultured microglial cells increased the level of $P2X_4R$ protein (Fig. 5*A*). Furthermore, intrathecal administration of IFN-γ increased the expression of $P2X_4R$ protein in the spinal cord of rats (Fig. 5*B*). In the dorsal horn, cells showing $P2X_4R$ immunofluorescence were double-labeled with OX-42 (Fig. 5*C*). Using $P2X_4R$-deficient mice ($p2rx4^{-/-}$), we found that the marked decrease in PWT induced by intrathecal administration of IFN-γ in wild-type C57BL/6J mice was significantly attenuated in $p2rx4^{-/-}$ mice ($P < 0.01$; Fig. 5*D*). In contrast to the PWT, IFN-γ-induced activation of microglia in the dorsal horn was similar in the 2 genotypes (Fig. 5*E*). This finding is consistent with our previous findings demonstrating that an antisense knockdown of $P2X_4R$ in the spinal cord fails to affect microglia activation (12). These results indicate that IFN-γR-mediated tactile allodynia depends on microglial $P2X_4R$.

Discussion

Growing evidence has revealed several microglial molecules involved in neuropathic pain (5–9). Although the expression levels or activities of these molecules are up-regulated in activated spinal microglia after nerve injury, they remain at low levels in resting microglia under normal conditions (9). By contrast, we show that in otherwise naive animals, spinal microglia express IFN-γRs in a cell-type-specific manner and that acute stimulation of these receptors alone induces a conversion

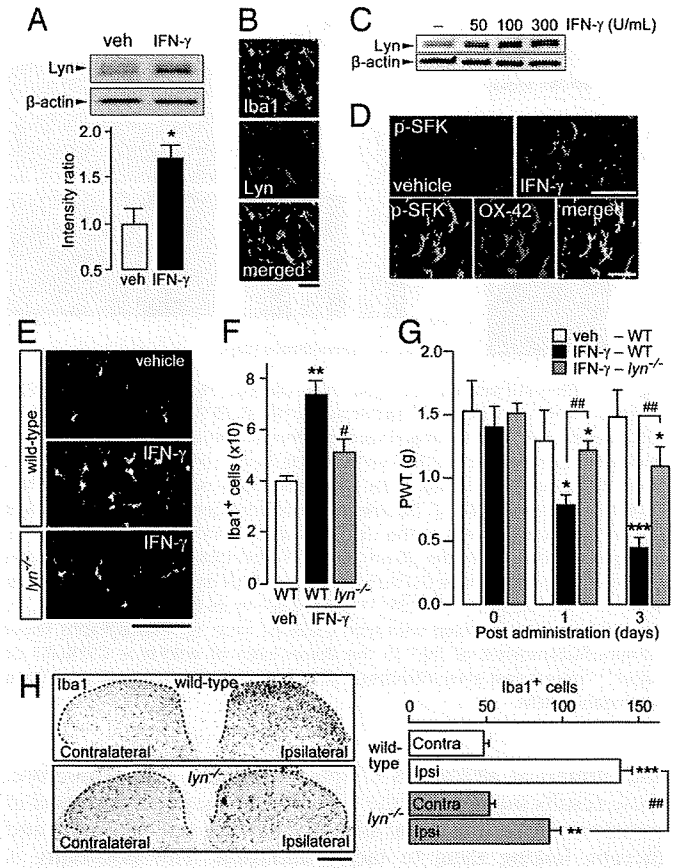

Fig. 4. Lyn is a crucial kinase mediating both IFN-γ- and nerve injury-induced activation of spinal microglia. (*A*) Western blot analysis of Lyn in spinal cord homogenates from rats treated intrathecally with IFN-γ (1,000 U). The relative values of Lyn protein were normalized to β-actin protein ($n = 3$; *, $P < 0.05$). (*B*) Double immunofluorescence labeling for Iba1 (green) and Lyn (red) in the dorsal horn of IFN-γ-treated rats (merged: yellow). (Scale bar, 30 μm.) (*C*) Lyn and β-actin proteins in a whole-cell lysate from primary cultured microglial cells treated with IFN-γ (50–300 U/ml) for 24 h. (*D*) Immunofluorescence of phospho-SFK (green) and double immunofluorescence labeling with OX-42 (red) in the dorsal horn of IFN-γ-treated rats (merged: yellow). (Scale bars, 80 μm [*Upper*] and 30 μm [*Lower*]). (*E*) Iba1 immunofluorescence in the dorsal horn of wild-type C57BL/6J and Lyn-deficient ($lyn^{-/-}$) mice 3 days after intrathecal administration of IFN-γ (10 U). (Scale bar, 80 μm.) (*F*) The number of $Iba1^+$ microglia in the dorsal horn [C57BL/6J: $n = 4$ (vehicle); $n = 6$ (IFN-γ); $lyn^{-/-}$: $n = 6$ (vehicle), $n = 5$ (IFN-γ); **, $P < 0.01$ vs. vehicle-treated wild-type C57BL/6J mice; ##, $P < 0.01$ vs. IFN-γ-treated wild-type C57BL/6J mice). (*G*) PWT after intrathecal administration of IFN-γ in wild-type C57BL/6J ($n = 6$) and $lyn^{-/-}$ ($n = 5$) mice (**, $P < 0.01$; ***, $P < 0.001$ vs. before IFN-γ injection; ##, $P < 0.01$ vs. IFN-γ-treated wild-type C57BL/6J mice). (*H*) Photographs show Iba1 immunofluorescence in the dorsal horn of C57BL/6J or $lyn^{-/-}$ mice 10 days after nerve injury and the number of $Iba1^+$ microglia in the dorsal horns ($n = 5$; **, $P < 0.01$; ***, $P < 0.001$ vs. contralateral side in wild-type C57BL/6J mice; ##, $P < 0.01$ vs. ipsilateral side in wild-type C57BL/6J mice). (Scale bar, 80 μm.) Data are mean ± SEM (*A*, *F*, *G*, and *H*).

of these cells into the activated state and produces long-lasting tactile allodynia. Our genetic approach revealed that IFN-γR deficiency results in a marked attenuation in spinal microglia activation and tactile allodynia in a model of neuropathic pain in which it was reported that IFN-γ levels were increased in the spinal cord (20). The attenuated microglia activation observed in IFN-γR-deficient mice seems to be in stark contrast to the phenotype observed in mice lacking $P2Y_{12}R$. $P2Y_{12}R$ is among the molecules expressed in microglia under normal conditions (30) and is implicated in neuropathic pain (32, 35); however, the loss of $P2Y_{12}R$ fails to affect nerve injury-induced morphological

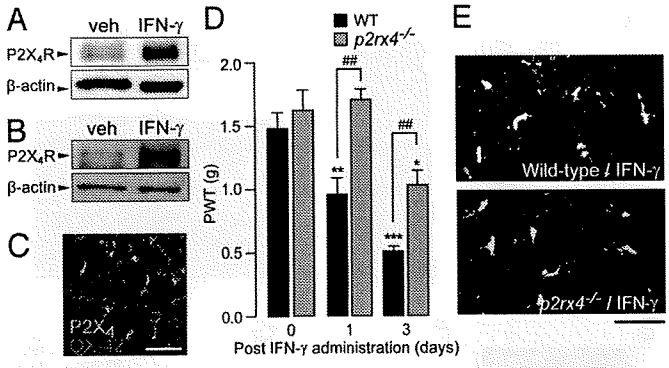

Fig. 5. IFN-γ-stimulated microglia show up-regulated expression of $P2X_4$ receptor, which is required for tactile allodynia. (*A*, *B*) Western blot analysis of $P2X_4$ receptor ($P2X_4R$) and β-actin proteins in a whole-cell lysate from cultured microglial cells treated with IFN-γ and vehicle for 24 h (*A*) and in homogenates from the spinal cord of rats 1 day after intrathecal administration of IFN-γ (1,000 U) or vehicle (*B*). (*C*) Double immunofluorescence labeling for $P2X_4R$ (green) and OX-42 (red) in the L5 dorsal spinal cord of IFN-γ-treated rats (merged: yellow). (Scale bar, 30 μm.) (*D*) PWT after intrathecal administration of IFN-γ (10 U) in wild-type C57BL/6J ($n = 6$) or $P2X_4R$-deficient (*p2rx4*$^{-/-}$) mice ($n = 5$). *, $P < 0.05$; **, $P < 0.01$; ***, $P < 0.001$ vs. before IFN-γ injection; ##, $P < 0.01$ vs. IFN-γ-treated wild-type C57BL/6J mice. (*E*) Photographs show immunofluorescence of Iba1 in the dorsal horn of wild-type C57BL/6J or *p2rx4*$^{-/-}$ mice 3 days after intrathecal IFN-γ injection. (Scale bar, 40 μm.) Data are mean ± SEM.

and numerical alterations of spinal microglia (32). Therefore, these results suggest that the IFN-γ/IFN-γR system is critical in transforming resting spinal microglia into the activated state and thereby linking them to tactile allodynia. This possibility is supported further by our evidence demonstrating that, in addition to cellular alterations, stimulation of resting spinal microglia by IFN-γ causes changes in their molecular profile (increased expression of Iba1, Lyn, and $P2X_4R$), changes that also occur in animal models of neuropathic pain (6–8, 12, 17). However, the fact that activation of spinal microglia after nerve injury was not completely eliminated in IFN-γR-deficient mice suggests that IFN-γR-mediated signaling, although important, is not the only mechanism underlying microglia activation and that there may be independent and/or cooperative mechanisms involving other signals (8).

Among numerous genes whose expression levels have been reported to be altered in microglia stimulated by IFN-γ (36), the present study identified Lyn tyrosine kinase to be up-regulated by IFN-γ and required for IFN-γR-dependent microglia activation. This kinase was up-regulated exclusively in microglia in a model of neuropathic pain (17) and was implicated in various cellular events in microglia (37–40). Previous work using Lyn-deficient mice also showed attenuated microglia activation evoked by β-amyloid peptide in the brain (39), supporting our notion that Lyn is critically involved in the molecular machinery underlying microglia activation. Consistent with the impaired neuropathic allodynia in mice lacking Lyn (17), these mice also were resistant to IFN-γ-induced tactile allodynia. We previously have indicated that Lyn kinase in microglia also controls the expression of $P2X_4R$ (17), a receptor that is crucial for tactile allodynia (6–8, 12, 23, 41–43). Interestingly, we further found that IFN-γ-stimulated spinal microglia allowed up-regulated expression of $P2X_4R$ and that the deletion of $P2X_4R$ blunted tactile allodynia, suggesting that IFN-γR-dependent tactile allodynia involves the $P2X_4R$. As shown previously (23), activation of $P2X_4R$ up-regulated in activated spinal microglia may lead to the release of bioactive factors such as BDNF, which causes hyperexcitability of dorsal horn neurons by reducing inhibition and converting $GABA_A$ receptor-mediated inhibition to excitation (23) and, in turn, produces tactile allodynia (12, 23). It is of particular interest that intrathecal delivery of IFN-γ to normal rats enhances the excitability of dorsal horn neurons evoked by innocuous stimulation in vivo (44, 45), possibly involving a reduction of GABAergic inhibitory control (45). Although such effects of IFN-γ have been considered a neuronally mediated phenomenon (44, 46, 47), our present findings indicating that spinal microglia are stimulated directly by IFN-γ administered spinally and contribute to IFN-γR-dependent pain hypersensitivity, together with recent evidence (6–9, 12, 23), suggest a mechanism in which spinal microglia are key intermediaries for the modulation of spinal pain processing by IFN-γ.

Our present study demonstrates that IFN-γR is a key element in the molecular machinery through which resting spinal microglia transform into the activated state that underlies the pathogenesis of neuropathic pain. On the other hand, the loss of IFN-γR did not change microglia morphology and number under normal conditions, despite the expression of IFN-γR in resting microglia. The lack of a phenotype in resting microglia also has been reported in the brains of IFN-γ-deficient mice (48). It thus is conceivable that this receptor may not affect the development and localization of microglia in the spinal cord and may not be activated under normal conditions. The lack of obvious activation of STAT1 in the normal spinal cord supports this notion. Together, these findings suggest that the attenuating effects of IFN-γR deficiency on the activation of spinal microglia in a model of neuropathic pain may be caused by the activation of this receptor by IFN-γ, which is elevated in the spinal cord after nerve injury (20). Because the loss of IFN-γR did not change basal pain sensitivity, our results also suggest that interfering with IFN-γR-mediated signaling in spinal microglia may be a novel approach to treating neuropathic pain without affecting physiological acute pain.

Materials and Methods

Detailed methods are presented in *SI Methods*.

Behavioral Studies. All experimental procedures were performed under the guidelines of Kyushu University. The PWT was measured using calibrated von Frey filaments in Wistar rats or mice (*ifngr*$^{-/-}$ [B6.129S7-*Ifngr1*^{tm1Agt}/J, The Jackson Laboratory], *lyn*$^{-/-}$ (49), *p2rx4*$^{-/-}$ (50), and their background wild-type control, C57BL/6J). The 3 knockout mouse lines were backcrossed to C57BL/6J mice for more than 10 generations. Minocycline was administered i.p. once a day from day 0 to day 7.

In Situ Hybridization. A digoxigenin-labeled antisense probe for the rat IFN-γR (NM_053783, sequence position 997-1713) was used.

Immunohistochemistry. Transverse L5 spinal cord sections (30 μm) were cut and processed for immunohistochemistry as described previously (12, 17). To visualize proliferating cells, BrdU (75 mg/kg, i.p.) was injected 22 h after intrathecal administration of IFN-γ; 2 h later, BrdU-treated rats were fixed by paraformaldehyde.

Microglial Culture. Rat primary cultured microglia were prepared in accordance with a method described previously (12, 51).

Western Blotting. Western blot analyses of Lyn and $P2X_4R$ expression in the membrane fractions from spinal cord segments L4-L6 and in whole-cell lysates of cultured microglial cells were performed in accordance with methods described previously (17).

Statistics. Statistical analyses of the results were made with Student's *t* test, Student's paired *t* test, or 1-way ANOVA with a post hoc test (Dunnett's multiple comparison test).

ACKNOWLEDGMENTS. We thank Dr. Tadashi Yamamoto and Dr. Joji Ando of the University of Tokyo for providing Lyn- and $P2X_4R$-knockout mice, respectively. This work was supported by grants from the Ministry of Education, Culture, Sports, Science and Technology of Japan (M.T. and K.I.). T.M. is a research fellow of the Japan Society for the Promotion of Science.

1. Baron R (2006) Mechanisms of disease: Neuropathic pain—a clinical perspective. *Nature Clinical Practice Neurology* 2:95–106.
2. Woolf CJ, Mannion RJ (1999) Neuropathic pain: Aetiology, symptoms, mechanisms, and management. *Lancet* 353:1959–1964.
3. Scholz J, Woolf CJ (2002) Can we conquer pain? *Nature Neuroscience* 5 Suppl:1062–1067.
4. Woolf CJ, Salter MW (2000) Neuronal plasticity: Increasing the gain in pain. *Science* 288:1765–1769.
5. Watkins LR, Milligan ED, Maier SF (2001) Glial activation: A driving force for pathological pain. *Trends Neurosci* 24:450–455.
6. Tsuda M, Inoue K, Salter MW (2005) Neuropathic pain and spinal microglia: A big problem from molecules in "small" glia. *Trends Neurosci* 28:101–107.
7. Marchand F, Perretti M, McMahon SB (2005) Role of the immune system in chronic pain. *Nature Reviews Neuroscience* 6:521–532.
8. Scholz J, Woolf CJ (2007) The neuropathic pain triad: Neurons, immune cells and glia. *Nature Neuroscience* 10:1361–1368.
9. Suter MR, Wen YR, Decosterd I, Ji RR (2007) Do glial cells control pain? *Neuron Glia Biology* 3:255–268.
10. Echeverry S, Shi XQ, Zhang J (2008) Characterization of cell proliferation in rat spinal cord following peripheral nerve injury and the relationship with neuropathic pain. *Pain* 135:37–47.
11. Pocock JM, Kettenmann H (2007) Neurotransmitter receptors on microglia. *Trends Neurosci* 30:527–535.
12. Tsuda M, et al. (2003) P2X4 receptors induced in spinal microglia gate tactile allodynia after nerve injury. *Nature* 424:778–783.
13. Jin SX, Zhuang ZY, Woolf CJ, Ji RR (2003) p38 Mitogen-activated protein kinase is activated after a spinal nerve ligation in spinal cord microglia and dorsal root ganglion neurons and contributes to the generation of neuropathic pain. *J Neurosci* 23:4017–4022.
14. Tsuda M, Mizokoshi A, Shigemoto-Mogami Y, Koizumi S, Inoue K (2004) Activation of p38 mitogen-activated protein kinase in spinal hyperactive microglia contributes to pain hypersensitivity following peripheral nerve injury. *Glia* 45:89–95.
15. Zhuang ZY, Gerner P, Woolf CJ, Ji RR (2005) ERK is sequentially activated in neurons, microglia, and astrocytes by spinal nerve ligation and contributes to mechanical allodynia in this neuropathic pain model. *Pain* 114:149–159.
16. Obata K, et al. (2007) Roles of extracellular signal-regulated protein kinases 5 in spinal microglia and primary sensory neurons for neuropathic pain. *J Neurochem* 102:1569–1584.
17. Tsuda M, et al. (2008) Lyn tyrosine kinase is required for P2X(4) receptor upregulation and neuropathic pain after peripheral nerve injury. *Glia* 56:50–58.
18. Inoue K (2006) The function of microglia through purinergic receptors: Neuropathic pain and cytokine release. *Pharmacol Ther* 109:210–226.
19. Farber K, Kettenmann H (2006) Purinergic signaling and microglia. *Pflugers Arch* 452:615–621.
20. Tanga FY, Nutile-McMenemy N, DeLeo JA (2005) The CNS role of Toll-like receptor 4 in innate neuroimmunity and painful neuropathy. *Proc Natl Acad Sci USA* 102:5856–5861.
21. Clark AK, Gentry C, Bradbury EJ, McMahon SB, Malcangio M (2007) Role of spinal microglia in rat models of peripheral nerve injury and inflammation. *European Journal of Pain (London, England)* 11:223–230.
22. Griffin RS, et al. (2007) Complement induction in spinal cord microglia results in anaphylatoxin C5a-mediated pain hypersensitivity. *J Neurosci* 27:8699–8708.
23. Coull JA, et al. (2005) BDNF from microglia causes the shift in neuronal anion gradient underlying neuropathic pain. *Nature* 438:1017–1021.
24. Keller AF, Beggs S, Salter MW, De Koninck Y (2007) Transformation of the output of spinal lamina I neurons after nerve injury and microglia stimulation underlying neuropathic pain. *Molecular Pain* 3:27.
25. Hanisch UK, Kettenmann H (2007) Microglia: Active sensor and versatile effector cells in the normal and pathologic brain. *Nature Neuroscience* 10:1387–1394.
26. Bach EA, Aguet M, Schreiber RD (1997) The IFN gamma receptor: A paradigm for cytokine receptor signaling. *Annu Rev Immunol* 15:563–591.
27. Maus U, et al. (2001) Monocytes recruited into the alveolar air space of mice show a monocytic phenotype but upregulate CD14. *American Journal of Physiology. Lung, Cellular, and Molecular Physiology* 280:L58–68.
28. Raivich G, et al. (1999) Neuroglial activation repertoire in the injured brain: Graded response, molecular mechanisms and cues to physiological function *Brain Research Brain Research Reviews* 30:77–105.
29. Sasaki Y, et al. (2003) Selective expression of Gi/o-coupled ATP receptor P2Y12 in microglia in rat brain. *Glia* 44:242–250.
30. Haynes SE, et al. (2006) The P2Y(12) receptor regulates microglial activation by extracellular nucleotides. *Nature Neuroscience* 9:1512–1519.
31. Raghavendra V, Tanga F, DeLeo JA (2003) Inhibition of microglial activation attenuates the development but not existing hypersensitivity in a rat model of neuropathy. *J Pharmacol Exp Ther* 306:624–630.
32. Tozaki-Saitoh H, et al. (2008) P2Y12 receptors in spinal microglia are required for neuropathic pain after peripheral nerve injury. *J Neurosci* 28:4949–4956.
33. Thomas SM, Brugge JS (1997) Cellular functions regulated by Src family kinases. *Annu Rev Cell Dev Biol* 13:513–609.
34. Salter MW, Kalia LV (2004) Src kinases: A hub for NMDA receptor regulation. *Nature Reviews Neuroscience* 5:317–328.
35. Kobayashi K, et al. (2008) P2Y12 receptor upregulation in activated microglia is a gateway of p38 signaling and neuropathic pain. *J Neurosci* 28:2892–2902.
36. Rock RB, et al. (2005) Transcriptional response of human microglial cells to interferon-gamma. *Genes and Immunity* 6:712–719.
37. Combs CK, Johnson DE, Cannady SB, Lehman TM, Landreth GE (1999) Identification of microglial signal transduction pathways mediating a neurotoxic response to amyloidogenic fragments of beta-amyloid and prion proteins. *J Neurosci* 19:928–939.
38. Tan J, Town T, Mullan M (2000) CD45 inhibits CD40L-induced microglial activation via negative regulation of the Src/p44/42 MAPK pathway. *J Biol Chem* 275:37224–37231.
39. Moore KJ, et al. (2002) A CD36-initiated signaling cascade mediates inflammatory effects of beta-amyloid. *J Biol Chem* 277:47373–47379.
40. Hooper C, Taylor DL, Pocock JM (2005) Pure albumin is a potent trigger of calcium signalling and proliferation in microglia but not macrophages or astrocytes. *J Neurochem* 92:1363–1376.
41. Nasu-Tada K, Koizumi S, Tsuda M, Kunifusa E, Inoue K (2006) Possible involvement of increase in spinal fibronectin following peripheral nerve injury in upregulation of microglial P2X(4), a key molecule for mechanical allodynia. *Glia* 53:769–775.
42. Tsuda M, et al. (2008) Fibronectin/integrin system is involved in P2X(4) receptor upregulation in the spinal cord and neuropathic pain after nerve injury. *Glia* 56:579–585.
43. Zhang Z, Zhang ZY, Fauser U, Schluesener HJ (2008) Mechanical allodynia and spinal up-regulation of P2X4 receptor in experimental autoimmune neuritis rats. *Neuroscience* 152:495–501.
44. Vikman KS, Siddall PJ, Duggan AW (2005) Increased responsiveness of rat dorsal horn neurons in vivo following prolonged intrathecal exposure to interferon-gamma. *Neuroscience* 135:969–977.
45. Vikman KS, Duggan AW, Siddall PJ (2007) Interferon-gamma induced disruption of GABAergic inhibition in the spinal dorsal horn in vivo. *Pain* 133:18–28.
46. Robertson B, et al. (1997) Interferon-gamma receptors in nociceptive pathways: Role in neuropathic pain-related behaviour. *NeuroReport* 8:1311–1316.
47. Vikman KS, Hill RH, Backstrom E, Robertson B, Kristensson K (2003) Interferon-gamma induces characteristics of central sensitization in spinal dorsal horn neurons in vitro. *Pain* 106:241–251.
48. Mount MP, et al. (2007) Involvement of interferon-gamma in microglial-mediated loss of dopaminergic neurons. *J Neurosci* 27:3328–3337.
49. Nishizumi H, et al. (1995) Impaired proliferation of peripheral B cells and indication of autoimmune disease in Lyn-deficient mice. *Immunity* 3:549–560.
50. Yamamoto K, et al. (2006) Impaired flow-dependent control of vascular tone and remodeling in P2X4-deficient mice. *Nat Med* 12:133–137.
51. Nakajima K, et al. (1992) Identification of elastase as a secretory protease from cultured rat microglia. *J Neurochem* 58:1401–1408.

SPINE Volume 34, Number 26, pp 2848–2857
©2009, Lippincott Williams & Wilkins

Tumor Necrosis Factor-Alpha and Its Receptors Contribute to Apoptosis of Oligodendrocytes in the Spinal Cord of Spinal Hyperostotic Mouse (*twy/twy*) Sustaining Chronic Mechanical Compression

Tomoo Inukai, MD, Kenzo Uchida, MD, PhD, Hideaki Nakajima, MD, PhD, Takafumi Yayama, MD, PhD, Shigeru Kobayashi, MD, PhD, Erisa S. Mwaka, MD, MMed, Alexander Rodriguez Guerrero, MD, and Hisatoshi Baba, MD, PhD

Study Design. To examine the distribution of apoptotic cells and expression of tumor necrosis factor (TNF)-α and its receptors in the spinal hyperostotic mouse (*twy/twy*) with chronic cord compression using immunohistochemical methods.

Objective. To study the mechanisms of apoptosis, particularly in oligodendrocytes, which could contribute to degenerative change and demyelination in chronic mechanical cord compression.

Summary of Background Data. TNF-α acts as an external signal initiating apoptosis in neurons and oligodendrocytes after spinal cord injury. Chronic spinal cord compression caused neuronal loss, myelin destruction, and axonal degeneration. However, the biologic mechanisms of apoptosis in chronically compressed spinal cord remain unclear.

Methods. The cervical spinal cord of 34 twy mice aged 20 to 24 weeks and 11 control animals were examined. The apoptotic cells were detected by the terminal deoxynucleotidyl transferase (TdT)-mediated dUTP-biotin nick end labeling (TUNEL) staining. The expression and the localization of TNF-α, TNF receptor 1 (TNFR1), and TNF receptor 2 (TNFR2) were examined using immunoblot and immnohistochemical analysis.

Results. The number of TUNEL-positive cells in the white matter increased with the severity of compression, which was further increased bilaterally in the white matter of *twy/twy* mice. Double immunofluorescence staining showed that the number of cells positive for TUNEL and RIP, a marker of oligodendrocytes, increased in the white matter with increased severity of cord compression. Immunoblot analysis demonstrated overexpression of TNF-α, TNFR1, and TNFR2 in severe compression. The expression of TNF-α appeared in local cells including microglia while that of TNFR1 and TNFR2 was noted in apoptotic oligodendrocytes.

Conclusion. Our results suggested that the proportion of apoptotic oligodendrocytes, causing spongy axonal degeneration and demyelination, correlated with the magnitude of cord compression and that overexpression of TNF-α, TNFR1, and TNFR2 seems to participate in apoptosis of such cells in the chronically compressed spinal cord.

Key words: apoptosis, oligodendrocytes, tumor necrosis factor (TNF)-α, spinal cord, spinal hyperostotic mouse (*twy/twy*), chronic compression. **Spine 2009;34:2848–2857**

Mechanical stimuli applied to the spinal cord can potentially induce profound and irreversible motor paresis secondary to dysfunction and loss of neurons. In particular, long-term and chronic mechanical compression of the spinal cord could gradually cause various pathologic changes of the neural tissue, such as reduced activity of surviving neuronal cells, neuronal degeneration, and demyelination of axons. A number of cadaver studies have examined the pathologic changes in chronically compressed spinal cords of patients with cervical spondylosis or ossified posterior longitudinal ligament showed demyelination as well as loss of axons in the white matter, and loss of neurons in gray matter.[1–3] However, the mechanism responsible for these pathologic changes remains elusive, partly because it is difficult to estimate these changes in human and animal experimental settings and there are few suitable animal models with progressive cord damage induced by long-term compression.

In a series of studies,[4–10] we examined this issue experimentally using the tiptoe-walking Yoshimura (*twy/twy*) mouse, a unique animal that develops spontaneous spinal cord compression. The *twy/twy* mouse is thus suitable for investigating the effects of chronic mechanical compression of the spinal cord, produced without any artificial manipulation of the cord.[4,11] Using these mice, we reported previously a progressive reduction in the number of anterior horn cells when the transverse remnant area of the spinal cord decreased to ≤70% of the control,[4,5] decreased usage of neurotrophins in autocrine and paracrine interactions,[6,8] and presence of accidental and apoptotic dying spinal cord cells.[12] However, the

From the Department of Orthopaedics and Rehabilitation Medicine, The University of Fukui, Fukui, Japan.
Acknowledgment date: February 18, 2009. Acceptance date: May 3, 2009.
The manuscript submitted does not contain information about medical device(s)/drug(s).
No funds were received in support of this work. No benefits in any form have been or will be received from a commercial party related directly or indirectly to the subject of this manuscript.
Supported, in part, by Grant-in-Aid to HB, HN and KU for General Scientific Research of the Ministry of Education, Science and Culture of Japan (grants numbers C15591571, B16390435, B18390411, and B19791023). This work was also supported in part by grants to HB from the Investigation Committee on Ossification of the Spinal ligaments, the Public Health Bureau of the Japanese Ministry of Labor, Health and Welfare (2005–2008).
The authors T.I. and K.U. have contributed equally to this work.
Address correspondence and reprint requests to Kenzo Uchida, MD, PhD, Department of Orthopaedics and Rehabilitation Medicine, The University of Fukui, Matsuoka Shimoaizuki 23–3, Eiheiji, Fukui 910-1193, Japan; E-mail: kuchida@u-fukui.ac.jp

Copyright © Lippincott Williams & Wilkins. Unauthorized reproduction of this article is prohibited.

correlation between spinal cord damage and neural cell apoptosis is not fully understood.[9]

Apoptosis of neural cells is an important tissue reaction that contributes to secondary damage after acute spinal cord injury.[13–17] There is evidence to suggest that tumor necrosis factor (TNF)-α can potentially trigger neural cell injury in the spinal cord.[18–20] TNF-α mediates several biologic and immunoregulatory responses in a variety of inflammatory diseases and trauma of the central nervous system,[21,22] including the spinal cord.[23,24] It is highly possible that both TNF receptor 1 (TNFR1) and TNF receptor 2 (TNFR2), which are members of the TNFR superfamily,[25,26] are involved in the cellular reactions mediated by TNF-α. It is highly possible that glial cells may also respond to neuronal cell death in *twy/twy* mouse, but this issue remains totally unknown.

The present study was thus designed to investigate the topographic distribution of glial cell apoptosis, particularly oligodendrocytes, within the chronically compressed *twy/twy* mouse spinal cord as well as the potential role of TNF-α, TNFR1, and TNFR2-mediated cell death cascade. The current communication is the first to describe the potential influence of apoptosis mediated through the TNF-α/TNFR pathway on chronically compressed spinal cord.

■ Materials and Methods

Animal Model

The present series of experiments were conducted in a total of 34 *twy/twy* mice (Central Institute for Experimental Animals, Kawasaki, Japan), aged 24 to 26 weeks with a mean body weight of 29.5 ± 7.3 g (±SD). Mutant *twy/twy* mice were maintained by brother-sister mating of heterozygous Institute of Cancer Research (ICR) mice (+/twy). The disorder is inherited in an autosomal recessive manner and the homozygous hyperostotic mouse is identified by a characteristic tip-toe walking at 6 to 8 weeks of age, although no congenital neurologic abnormalities are detected at that age. The *twy/twy* mouse exhibits spontaneous calcified deposits posteriorly at the C1–C2 vertebral level, producing a variable degree of compression of the spinal cord between C2 and C3 segments (Figure 1A). The calcified mass grows progressively with age particularly in the atlantoaxial membrane, causing profound motor paresis later in life. ICR mice, age-matched with the *twy/twy* mice, were used as controls. Table 1 summarizes the number of mice used in the study. The experimental protocol was approved by the Ethics Committee for Animal Experimentation of our University.

To assess the effect of compression in the longitudinal direction, 3 segments of the cervical spinal cord were selected[5,6]; the segment immediately rostral to the compressive lesion between C1 ventral and C2 dorsal roots (rostral site); the site of maximal compression between C2 and C3 dorsal roots (maximally compressed site); and the segment immediately caudal to the compression lesion between C3 and C4 dorsal roots (caudal site). The length from the caudal site to the rostral site of the spinal cord assessed histologically was on average 3150 μm. To assess the effects of various degrees of spinal cord compression, the maximally compressed transverse remnant area of the spinal cord (TRAS) was used as a parameter of the magnitude of external compression. The ratio of the TRAS in the *twy/twy* mouse to that of the control ICR mouse was designated as TRAS%. We defined TRAS% ≤70% as compressed spinal cord in *twy/twy* mice.[4,5] Mice were divided into 2 groups based on the value of TRAS%: moderate compression group (TRAS% between 50% and 70%, Figure 1B); and severe compression group (TRAS% ≤50%, Figure 1C).

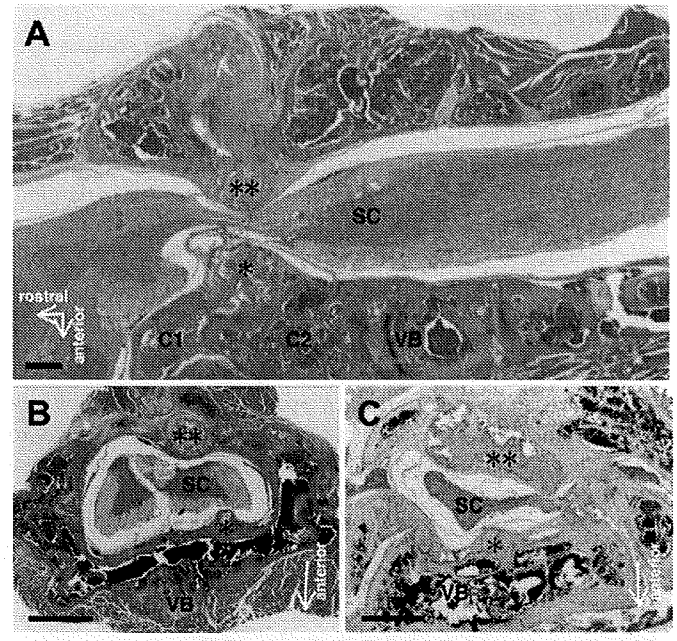

Figure 1. Photomicrographs showing sagittal sections of the spinal cord between the medulla oblongata and C4 spinal cord segment of 24-week-old *twy/twy* mouse (**A**; C1, atlas; C2, axis; Hematoxylin and eosin staining). Calcified lesions (*, **) emanating from the posterior longitudinal ligament and atlantoaxial membrane significantly compress the spinal cord *vis a fronte* (*) and *vis a tergo* (**), respectively. Transverse sections of the spinal cord show moderate compression (**B**) at the maximally compressed site at C1–C2 vertebral levels in 24-week-old mouse and severe compression (**C**) at the same site at the same age. SC indicates spinal cord; VB, vertebral body. Scale bars = 500 μm in (**A**, and 200 μm in **B**, **C**.

Table 1. Number of Mice Used in the Present Study

		twy/twy Mice	
	ICR Mice	Moderate Compression (TRAS% >50% but ≤70%)	Severe Compression (TRAS% ≤50%)
TUNEL staining (paraffin sections)	2	4	4
Electron microscopy	2	2	2
TUNEL and double immunofluorescence staining (frozen sections)	2	4	4
Evaluation of apoptotic signal in oligodendrocytes (frozen sections)	2	4	4
Immunoblot analysis	3	3	3

ICR mice indicates control mice; TRAS, transverse remnant area of the spinal cord.

Copyright © Lippincott Williams & Wilkins. Unauthorized reproduction of this article is prohibited.

TUNEL Staining

After anesthesia with intraperitoneal injection of sodium barbiturate (0.05 mg/g body weight), the animal was perfused intracardially using 50 mL phosphate buffered saline (PBS; at 4°C) followed by 100 mL of 4% paraformaldehyde in 0.1 M PBS (pH 7.6). Immediately after perfusion, the cervical cord was removed *en bloc*, postfixed, and then embedded in paraffin. Samples were cut in 4-μm thick serial transverse sections. Deoxyribonucleic acid fragmentation was detected by the terminal deoxynucleotidyl transferase (TdT)-mediated dUTP-biotin nick end labeling (TUNEL) method using the ApopTag Peroxidase In Situ Apoptosis Detection kit (Chemicon International, Temecula, CA). After deparaffinization and hydration, sections were treated with 20 μg/mL of proteinase K in 0.1 mol/L of TRIS buffer (pH 8.0) at room temperature for 15 minutes to strip nuclei of tissue sections. The procedures used were performed as described in the kit manual. The reaction with TdT was terminated by washing the sections with stop-wash buffer for 30 minutes at 37°C. Antidigoxigenin peroxidase was then applied for 30 minutes at room temperature. Color was developed using 3, 3′-diaminobenzidine tetrachloride. Finally, sections were counterstained with methyl green.

Double Immunofluorescence Staining

To identify the type of apoptotic cells, double immunofluorescence staining was performed using frozen sections. The cervical spinal cord was removed as described above and embedded in Tissue-Tek (optimal cutting temperature compound 4583, Sakura FineTechnical, Tokyo) and frozen at −80°C. Serial 25-μm thick transverse frozen sections were treated with 0.1 M TRIS-HCl buffer (pH 7.6) containing 0.3% Triton-X-100 for another 24 hours to allow reaction of the cell membrane with antibodies. Sections were then subjected to TUNEL using an ApopTag Plus Fluorescein *In Situ* Apoptosis Detection kit (Chemicon International). The procedures used were performed exactly as described in the kit manual. The reaction with TdT was terminated by washing the sections with stop-wash buffer for 30 minutes at 37°C. Antidigoxigenin-Fluorescein was applied for 30 minutes at room temperature. After that, the sections were then incubated with antioligodendrocyte monoclonal antibody (RIP, 1:100,000, mouse IgG; Chemicon International) for oligodendrocytes, antineuronal nuclei monoclonal antibody (NeuN, 1:400, mouse IgG; Chemicon International) for neurons, antiglial fibrillary acidic protein monoclonal antibody (GFAP, 1:400, mouse IgG; Chemicon International) for astrocytes, and antimicroglia monoclonal antibody (OX-42, 1:400, mouse IgG; Chemicon International) for microglia diluted in Antibody Diluent with Background Reducing Components (Dako Cytomation, Carpenteria, CA) at 4°C overnight. The sections were then incubated with goat antimouse Alexa Flour 568/fluorescein-conjugated antibody (1:250; Molecular Probes, Eugene, OR). The immunostained cells were visualized under confocal microscope equipped with a 15-mWatt crypton argon laser (model TCS SP2, Leica Instruments, Nusslosh, Germany). The 488- and 543-nm lines of an argon/helium-neon laser were used for fluorescence excitation.

To determine the relationship between TNF-α/TNFR combination pathway and apoptosis of oligodendrocytes in *twy/twy* mice, double staining was performed in a manner similar to that described above. Serial 25-μm thick transverse frozen sections were incubated overnight with OX-42 (1:400, mouse IgG; Chemicon International), GFAP (1:400, mouse IgG; Chemicon International), RIP (1:100,000, mouse IgG; Chemicon International), anti-TNF-α (1:100, gout IgG; Santa Cruz Biotechnology, Santa Cruz, CA), anti-TNFR1 (1:100, rabbit IgG; Santa Cruz Biotechnology), anti-TNFR2 (1:100, rabbit IgG; Santa Cruz Biotechnology), and antiactive caspase-3 (1:100, rabbit IgG; Chemicon International) diluted in antibody diluent with background reducing components (Dako Cytomation) at 4°C. The secondary antibodies were goat antimouse Alexa Flour 568/fluorescein-conjugated antibody (1:250; Molecular Probes, Eugene, OR), donkey antigout antibody Alexa Flour 488/fluorescein-conjugated antibody (1:250; Molecular Probes), and goat antirabbit antibody Alexa Flour 488/fluorescein-conjugated antibody (1:250; Molecular Probes). The immunostained cells were visualized under a confocal laser scanning microscope (model TCS SP2, Leica Instruments).

Immunoblot Analysis

After cardiac arrest, the cervical spinal cord was immediately removed *en bloc* and stored in liquid nitrogen. The sample was solubilized in RIPA buffer (50 mmol/L pH 7.5 TRIS-HCl, 150 mmol/L NaCl, 1% Triton X-100, 0.5% sodium deoxycholate, 20 μg/mL leupeptine, and 1 mmol/L phenylmethylsulfonylfluoride), homogenized and then stored at −80°C. The protein concentration was analyzed by Bio-Rad DC protein assay kit (No. 500–0116, Bio-Rad Laboratories, Hercules, CA). Laemmli sodium dodecylsulfate buffer samples containing proteins were boiled and subjected to immunoblot analysis. Total protein (80 μg/lane) was subjected to sodium dodecylsulfate polyacrylamide gel (15%) electrophoresis and transferred onto polyvinylidene difluoride membrane (PE Applied Biosystems, Foster city, CA) for 70 minutes in a semidry blot apparatus. The membranes were then washed twice in PBS containing 0.05% Tween 20, and then blocked by 5% skim milk in PBS for 1 hour, subsequently reacted with anti-TNF-α (1:200, rabbit IgG; Santa Cruz Biotechnology), anti-TNFR1 (1:200; Santa Cruz Biotechnology), anti-TNFR2 (1:200; Santa Cruz Biotechnology), and antiactive caspase-3 (1:500; Chemicon International) diluted overnight at 4°C sequentially by antirabbit IgG antibody and avidin-biotinylated peroxidase complex (1:200; Envision System-HRP Labeled Polymer, Dako Cytomation) for 3 hours. After triple washing in PBS, the membrane was sunk in the ECL for 1 minute to take a radiograph film for visualization of peroxidase activity. This immunoblot analysis was described in detail in our previous publications.[8–10]

Transmission Electron Microscopy

The cervical spinal cord including the above-described 3 levels of *twy/twy* mice and the same levels of control ICR mice were fixed with 2.5% glutaraldehyde and 2.5% paraformaldehyde, followed by late-fixation in 1% osmium tetroxide for 2 hours. Fixed specimens were dehydrated in a graded series of alcohol, embedded in epoxy resin and polymerized at 60°C for 2 days. Ultrathin sections were cut by ultramicrotome, stained with uranyl acetate and lead citrate, and examined with a Hitachi H-7650 transmission electron microscope (TEM; Hitachi, Tokyo).

Cell Counts and Statistical Analysis

The number of dark-gray colored TUNEL-positive cells was counted in the anterior, lateral, and posterior columns, as well as anterior and posterior horns at each segment of the cervical spinal cord. Four cross-sections were randomly selected out of 10 to 15 sections from each segment of each mouse (4 *twy/twy* mice at each level of spinal cord compression and 2 ICR mice). Similarity in double immunofluorescence staining, the number

Copyright © Lippincott Williams & Wilkins. Unauthorized reproduction of this article is prohibited.

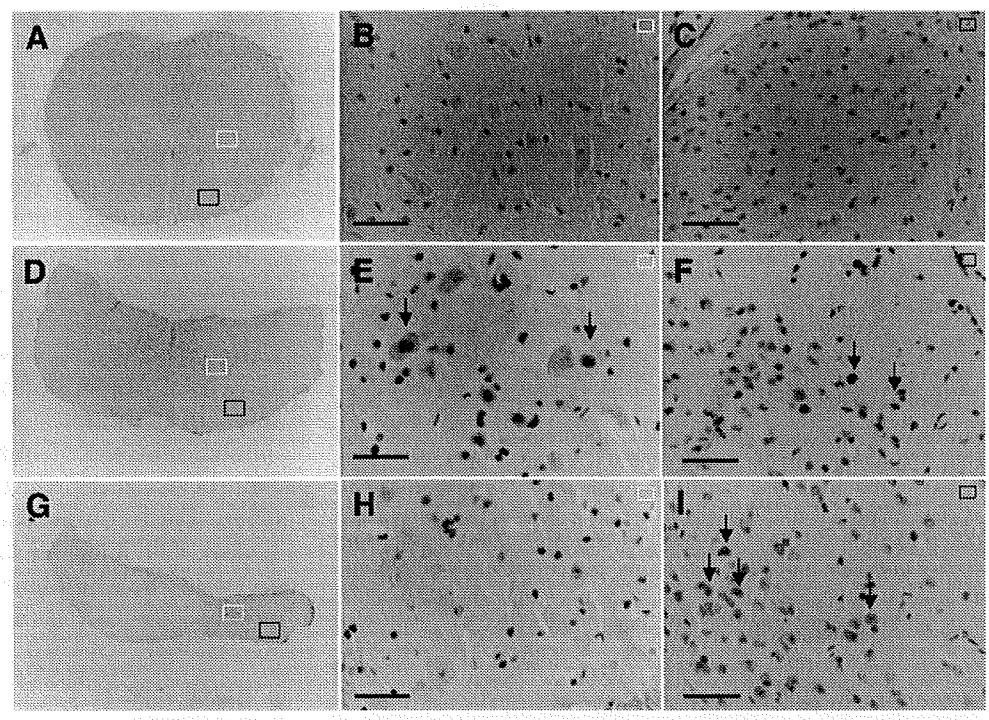

Figure 2. Photomicrographs showing findings of terminal deoxynucleotidyl transferase (TdT)-mediated dUTP nick-end labeling (TUNEL) staining in control ICR (**A–C**) and *twy/twy* (**D–I**) mice. Middle row: spinal cord of a *twy/twy* mouse with a transverse remnant area of the spinal cord (TRAS) of 50% to 70%, bottom row: spinal cord of a *twy/twy* mouse with a TRAS of ≤50%. Left column (**A, D, G**): photomicrographs taken by a roupe (×3). The white rectangular area (anterior horn of the gray matter) and black rectangular area (anterior column of the white matter) are enlarged in the same row in the middle and right columns, respectively. Black arrows: representative TUNEL-positive cells. Scale bars = 50 μm.

of TUNEL- (green) labeled cells and the number of TUNEL- and RIP-(red) double labeled cells (yellow) was counted on the white matter using a fluorescent microscopy. The Mann-Whitney *U* test was used to compare the numbers of TUNEL-positive cells in each region in the moderate and severe compression groups. All values were expressed as mean ± SEM. A $P < 0.05$ denoted the presence of a significant difference between groups.

■ Results

Histologic Evaluation of Apoptosis in the twy/twy Mouse Spinal Cord and Transmission Electron Microscope Findings

Topographic distribution of TUNEL-positive cells in the chronically compressed spinal cord of *twy/twy* mice examined by the TUNEL method is shown in Figure 2. No TUNEL-positive cells were identified in both the gray and white matters of the control ICR mouse spinal cord (Figures 2A–C). In contrast, a number of TUNEL-positive cells were found in the anterior horn (Figure 2E), posterior horn and anterior column (Figure 2F), lateral as well as posterior columns in the *twy/twy* mice with moderate compression (Figures 2D–F). In comparison, fewer TUNEL-positive cells were found in the severe compression group particularly in the anterior horn (Figures 2G, H), though these cells were abundant in the anterior (Figure 2I), lateral and posterior columns.

Figure 3 shows the results of comparative quantitative analysis of TUNEL-positive cells in the posterior and anterior horns, and posterior, lateral and anterior columns at the spinal cord level rostral to compression (Figure 3A), maximal compression (C1–C2 vertebral level, Figure 3B), and caudal to compression (Figure 3C). Fewer such cells were noted in the gray matter at the level of maximal compression (Figure 3B). In the spinal cord

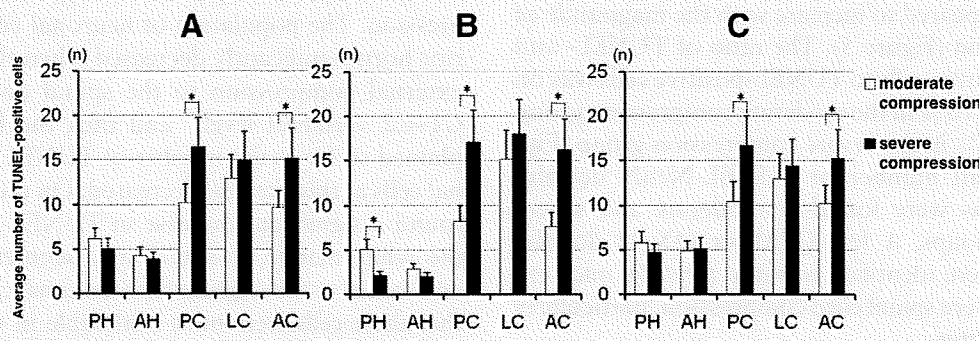

Figure 3. Quantification of distribution of TUNEL-positive cells at 3 representative segments (**A**, site rostral to maximally compressed segment; (**B**,) site of maximal compression at C1–C2 vertebral level; (**C**,) site caudal to the maximal compression) of the *twy/twy* mouse with moderate and severe external compression. Abscissa: representative anatomic site; PH indicates posterior horn; AH, anterior horn; PC, posterior column; LC, lateral column; AC, anterior column of the spinal cord. Ordinate: the number of number of TUNEL-positive cells. The number of TUNEL-positive cells was higher in the white matter (PC, AC) in severe compression compared with moderate compression. There appeared significant decrement in the number of TUNEL-positive cells in the gray matter (PH) in the maximally compressed spinal cord segment (middle graph, **B**). Data are mean ± SEM of number of mice indicated in Table 1. *$P < 0.05$.

Copyright © Lippincott Williams & Wilkins. Unauthorized reproduction of this article is prohibited.

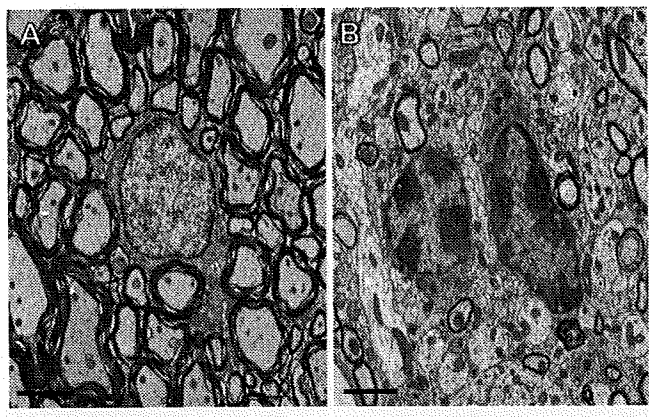

Figure 4. Transmission electron micrographs showing glia-like cells in the white matter of the control ICR mouse (**A**) and *twy/twy* mouse in the maximally compressed spinal cord segment (**B**) with severe compression. The glia-like cell in ICR mouse shows absence of apoptosis (**A**) but in the *twy/twy* mouse, the glia-like cell shows aggregation of nuclear chromatin into dense and sharply delineated masses despite preservation of cytoplasmic organelles, suggestive of cell apoptosis (**B**). Scale bars = 2 μm.

of *twy/twy* mice with severe compression, the number of TUNEL-positive cells was significantly lower in the posterior horn at the segment of maximal compression (Figure 3B), and was also significantly higher in the white matter, particularly, posterior and anterior columns in all 3 spinal cord segments (Figures 3A–C), compared with moderate compression.

TEM examination showed a significant number of apoptotic glia-like cells in the white matter, particularly in the maximally compressed segment of the spinal cord with severe compression. TEM also showed accumulation of nuclear chromatin into dense, finely delineated masses, together with preservation of cytoplasmic organelles (Figure 4B). The presence of TUNEL-positive cells confirmed that these were apoptotic cells. In contrast, no such apoptotic cells were seen in control ICR mice (Figure 4A).

Findings in Double Immunofluorescence Staining

In *twy/twy* mice, most TUNEL-positive cells were also RIP-positive, and the number of TUNEL-RIP double-positive cells appeared to increase with the magnitude of cord compression (Figure 5). The ratio of TUNEL- and RIP-double positive cells to TUNEL-positive cells was on average 59% ± 18% in the moderate compression group and 78% ± 14% in the severe compression group (Figure 5J). A small number of TUNEL-NeuN double-positive neurons were found in moderate and severe compression groups. A few GFAP or OX-42 double-positive cells were identified in some *twy/twy* mice examined with severe spinal cord compression, particularly in the white matter.

TNF-α-Mediated Apoptosis in the twy/twy Mouse Spinal Cord

Next, we evaluated the relationship between TNF-α/TNFR pathway and apoptosis in *twy/twy* mouse spinal cord by immunoblot analysis. Overexpression of TNF-α, TNFR1, and TNFR2, and activation of caspase-3, a marker of apoptosis, was evident in *twy/twy* mouse spinal cord compared with ICR mouse (Figure 6). Semiquantitative immunoblot analysis showed increased immunoreactivity to TNF-α, TNFR1, and TNFR2, and activated-caspase-3, with increase in the magnitude of spinal cord compression.

In *twy/twy* mice with severe cord compression (TRAS% ≤50%), double-staining for TNF-α and OX-42, GFAP and RIP was identified (Figure 7), which was scattered in the compressed cord particularly in the white matter. In sections double-stained for TNFR1, TNFR2, and activated-caspase-3 with RIP, a number of double-stained cells were identified among the abundant oligodendrocytes in the white matter of *twy/twy* mouse with severe cord compression (Figure 8). Expression of TNF-α, TNFR1, TNFR2, and activated-caspase-3 was noted in the abundant oligodendrocytes in *twy/twy* mouse.

■ Discussion

A number of investigators have attempted to characterize the pathologic features of chronically compressed spinal cords of patients with cervical myelopathy secondary to spondylosis or ossified posterior longitudinal ligament.[1–3] These studies reported the presence of exfoliation of anterior horn neurons with progressive spongy degeneration and demyelination in the white matter in areas of spinal cord mechanical compression. In our previous publications, we observed a significant reduction in the number of remaining surviving neurons (Nissl stain-positive motoneurons) when the TRAS% of the *twy/twy* spinal cord decreased to ≤70% of the control.[4,5] Furthermore, we also reported that the extent of demyelination and Wallerian degeneration in the white matter increased proportionately with the magnitude of spinal cord compression.[7] In the present study, we found significant decrement in the number of TUNEL-positive cells in the posterior horn of the gray matter in the maximally compressed spinal cord segment in severe compression. The population of neuronal cells in the posterior horn significantly decreased when the magnitude of external compression to the spinal cord increased at C1–C2 vertebral level,[5] and thus the findings are explained so far as the number of TUNEL-positive neuronal cells at this site also decreased. On the other hand, we found a significant increase in TUNEL-positive cells in the white matter, in spinal cord segments both rostral and caudal to the segment with maximal compression, and that these cells were most noticeable in the anterior and posterior columns of the spinal cords of *twy/twy* mice with severe compression. Although TUNEL staining is not specific to apoptotic cells,[27] because the staining is also positive for necrotic cells, our observation suggests that neuronal loss in anterior horn, after gray matter atrophy or together with spongy degeneration and demyelination in

Copyright © Lippincott Williams & Wilkins. Unauthorized reproduction of this article is prohibited.

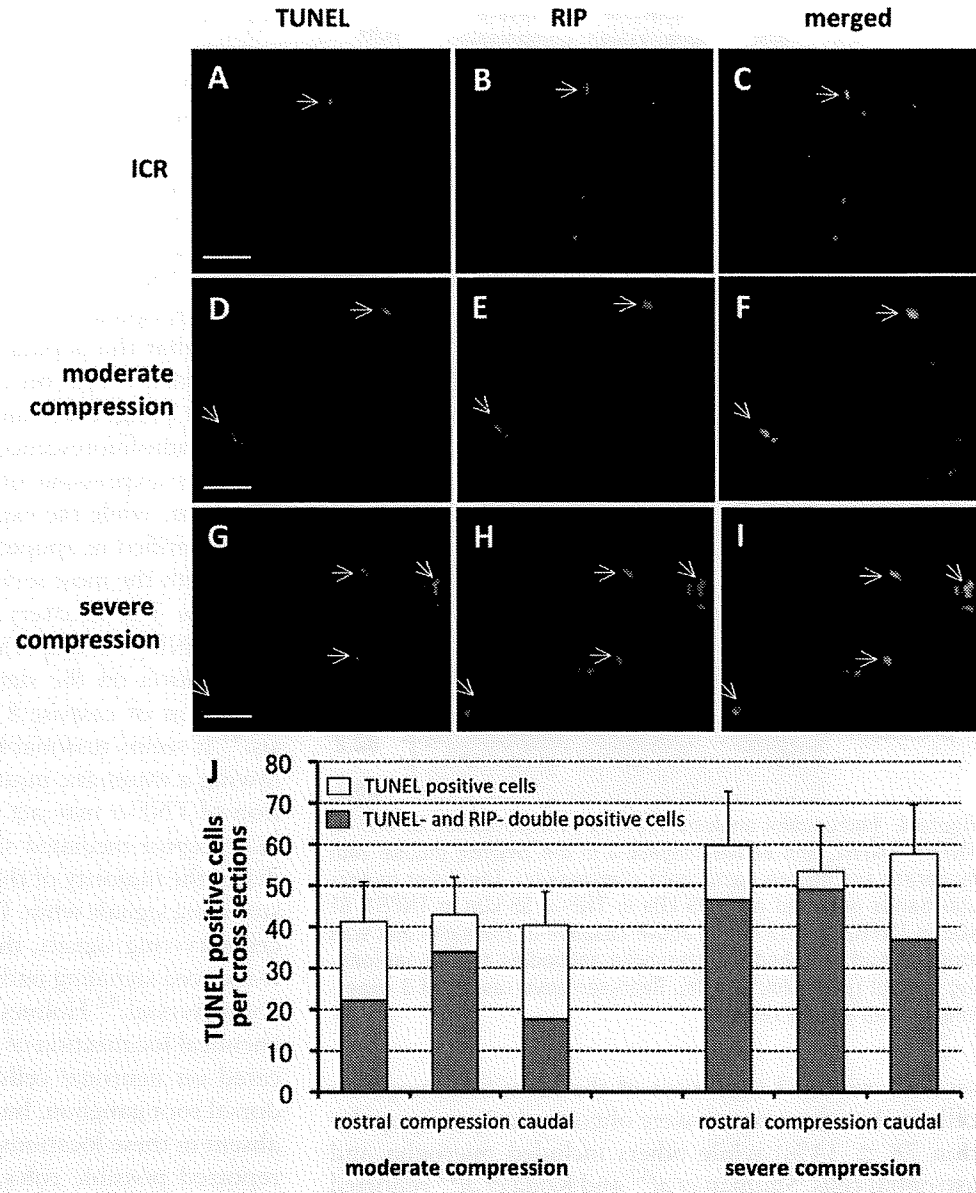

Figure 5. Photomicrographs of double immunofluorescence staining of TUNEL-positive cells with antioligodendrocyte monoclonal antibody (RIP) in the anterior column of the *twy/twy* mouse at maximally compressed C1–C2 spinal cord segment. White arrows in (**A–I**) indicate colocalization of TUNEL and RIP. Overlap of markers appears as yellow color in the middle and bottom rows. Note the increased number of double-stained oligodendrocytes (white arrows) in *twy/twy* mouse with severe compression compared with that of moderate compression. Scale bars = 50 μm. **J**, shows the ratio of TUNEL- and RIP-double positive cells (yellow) to the total number of TUNEL-positive cells (green) in each moderate and severe compression group at 3 representative segments in the white matter (posterior column, lateral column, anterior column). The percentages of TUNEL and RIP double-positive cells out of the total number of TUNEL-positive cells was on average 59% in the moderate compression group and 78% in the severe compression group.

the white matter of the *twy/twy* mouse spinal cord is likely to be due to apoptotic death of neurons and glia.

Apoptosis is an active form of cell death that occurs in a variety of physiologic and pathologic conditions, such as damage to the central nervous system caused by ischemia,[28,29] neuronal degenerative diseases,[30] and viral encephalitis.[31] After spinal cord injury, apoptosis of neurons and glial cells occurs rapidly at the level and vicinity of the traumatic injury, thus contributing to a secondary pathologic cascade of neural injury. Several groups have concluded that neuronal cell apoptosis is the underlying process of spinal cord damage after traumatic injury.[13–15] Our group suggested previously the role of mitogen activated protein-kinase cascade in neuronal cell apoptosis of *twy/twy* mice in addition to other yet unknown mechanism(s).[16] In spinal cord injury, apoptotic oligodendrocytes are found along the spinal cord longitudinal axis both proximally and caudally far from the level of injury, but most significantly at and around the level of injury.[15,17,29] Liu *et al*[15] reported that the initial damage of neurons and oligodendrocytes occurred extensively in the area of direct trauma and that 7 days later, the second wave of injury occurred mainly in the form of apoptotic oligodendrocytes in the white matter proximally and caudally far from the level of direct injury. Several chemical and circulatory disturbances, in addition to other yet unknown mechanisms could contribute to such extensive apoptosis of oligodendrocytes. Crowe *et al*[13] reported that apoptosis of oligodendrocytes occurring distal to the injury site in a spinal cord injury model was possibly due to a lack of neurotrophic factors after axonal damage. It is highly probable for oligodendrocytes and other neural cells to undergo cellular death through this neurotrophin-deficient apoptosis mechanism, and we have reported recently the presence of neurotrophin deficiency-related cell death, including apoptosis, in acute spinal cord injury.[32] Apoptosis of oligodendrocyte correlates significantly with delayed axonal demyelination after spinal cord injury.[29] In the current study in *twy/twy* mouse model, immunocytochemistry of double-stained

Copyright © Lippincott Williams & Wilkins. Unauthorized reproduction of this article is prohibited.

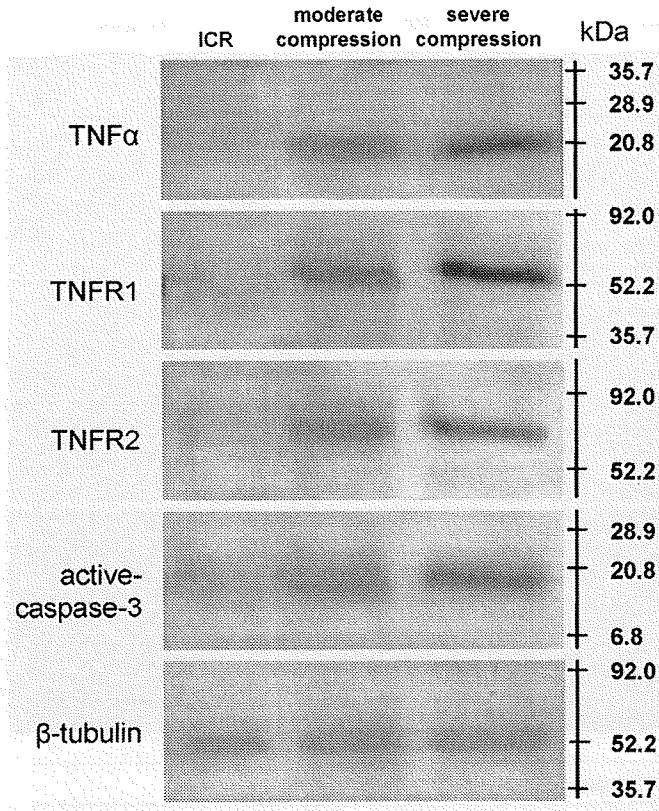

Figure 6. Immunoblot analysis showing overexpression of TNF-α, TNFR1, TNFR2, and active-caspase-3 in the *twy/twy* mouse with moderate and severe spinal cord compression. The major molecular bands detected were 19 kDa in TNF-α, 55 kDa in TNFR1, 81 kDa in TNFR2, and 17 kDa in active-caspase-3. The same blot was stripped and reprobed with β-tubulin antibodies as internal loading control (β-tubulin; 52 kDa). Representative results of 3 experiments with similar results.

sections revealed that most of the identified apoptotic cells in the white matter were oligodendrocytes (population 78 ± 14%) while others included microglia and astroglial cells. Shuman *et al*[33] and Koda *et al*[27] reported similar findings in different trauma models of spinal cord injury. Though insignificant when compared with the acute spinal cord injury, the longitudinally diffuse and extensive pattern of oligodendrocyte apoptosis in *twy/twy* mouse may be similar to the secondary damage process observed after acute trauma, and it was very interesting that increment in the number of apoptotic cells in this mouse model was proportional to the magnitude of chronic external compression.

A variety of signal transduction pathways are involved in the complex process of apoptosis.[12,34] Caspases are a family of cysteine proteases that play important roles in the effector phase of apoptosis and are activated through intrinsic and extrinsic pathways. Previous studies reported that spinal cord injury resulted in the induction of apoptosis mediated by caspase-3[35] and increased expression of the death receptors, especially Fas and p75 receptors.[36] The p75 neurotrophin receptors play a role in not only the promotion of neuronal cell death[37] but also neuronal survival.[38] On the other hand, the extrinsic pathway is initiated by ligand of cell surface death receptors belonging to the TNF/nerve growth factor receptor superfamily.[39] Recent studies have described overexpression of TNF-α in apoptotic neuronal and glial cells including microglia in spinal cord injury and suggested it was the cytokine that triggers oligodendrocyte apoptosis, though the source of this TNF-α in injured spinal cord was not clear.[19,40] A previous study suggested that activated microglia secrete various cytotoxic factors including TNF-α in response to axonal regeneration and induce apoptosis of oligodendrocytes. It was also reported that the population of apoptotic cells following spinal cord contusion comprised oligodendrocytes and possibly phagocytic microglia or macrophages.[33] Double immunofluorescence staining in this study also indicated the expression of TNF-α in local cells including microglia, while the expression of TNFR1 and TNFR2 was identified in apoptotic oligodendrocytes in the segment with the most severe cord compression in the *twy/twy* mice. The discovery and studies of a "death domain" in the TNFR1 and in other related receptors has revealed information on the signaling pathways leading to the activation of caspase-8 and caspase-3, before apoptosis.[41] It seems reasonable to suggest, therefore, that following a traumatic injury to the spinal cord, accumulation of TNF-α may act to initiate an apoptotic cascade *via* receptor-mediated signaling. Although TNFR1 mediates the majority of the apoptotic effects as well as cell surviving signals while TNFR2 predominantly transmits cell-surviving signals, their locations and roles in TNF-α-induced signaling pathway are still not elucidated and controversial.[42] Holmes *et al*[25] described immunocytochemical localization of these receptors: TNFR1 was located on neuronal cells and afferent fibers within the dorsal root ganglion, but TNFR2 immunoreactivity was absent in these locations. On the other hand, Yan *et al*[26] reported possible roles of expression of TNFR1 and TNFR2 in adult rat spinal cord injury. They reported overexpression of TNFR1 and TNFR2 in the spinal cord and that such expression was located on neurons, astrocytes, and oligodendrocytes after spinal cord injury. In chronic spinal cord compression, we found overexpression of both TNFR1 and TNFR2 primarily in oligodendrocytes and the number of those receptor-positive oligodendrocytes increased proportionately with the increased magnitude of mechanical compression in the *twy/twy* mouse. Although this source was not demonstrated in the present study and mechanisms other than those involving TNF-α and TNFRs (TNFR1 and TNFR2) pathway exist for apoptosis of oligodendrocytes,[33] the above results and those of the present study suggest the involvement of certain mechanisms in upregulation of inflammatory cytokines, including TNF-α, and that mechanical compression-induced expression of TNFR1 and TNFR2 may closely contribute to apoptosis, particularly that of oligodendrocytes in *twy/twy* mouse spinal cord with severe compression, a model that simulates cervical compressive myelopathy.

Copyright © Lippincott Williams & Wilkins. Unauthorized reproduction of this article is prohibited.

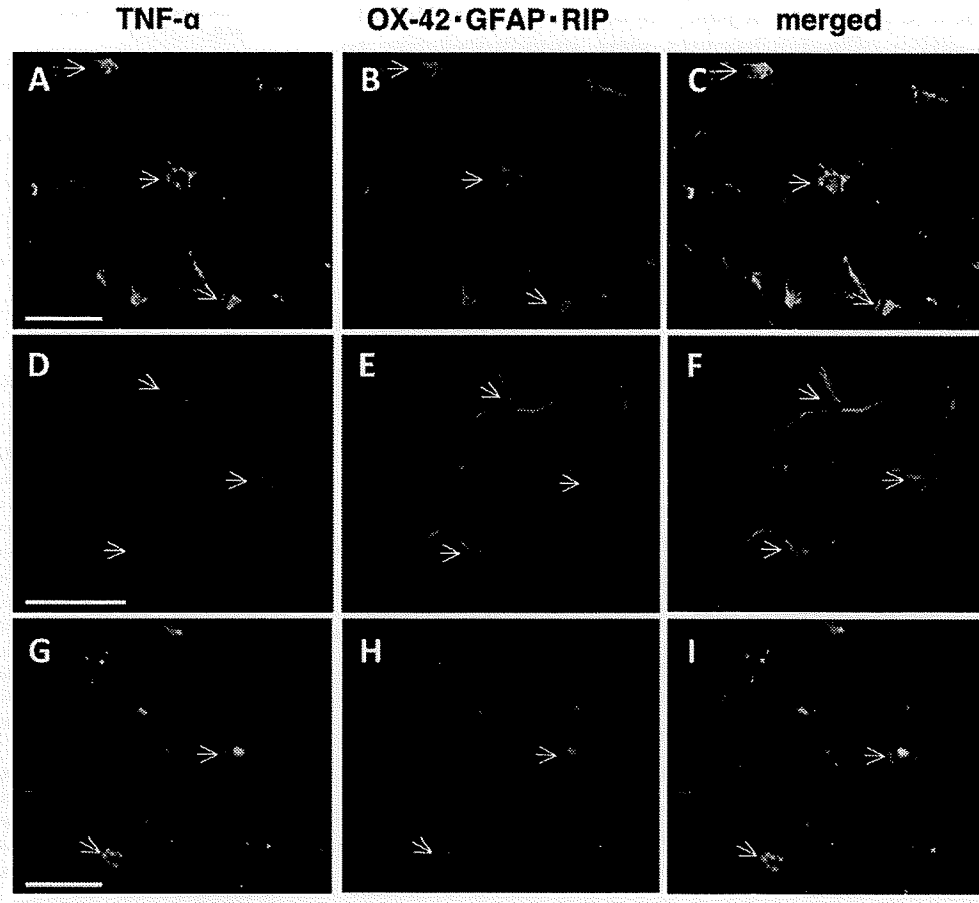

Figure 7. Photomicrographs showing double immunostaining for TNF-α and immunoreactivity for microglia OX-42, astrocyte GFAP and oligodendrocyte RIP in the anterior column at spinal cord level of maximal compression in *twy/twy* mice with severe compression. White arrows in A-I: colocalization of TNF-α, OX-42, GFAP and RIP. Overlap of the markers appears yellow in the third rows. Note the expression of TNF-α in microglia, astrocytes, and oligodendrocytes. Scale bars = 20 μm (**A–F**), 10 μm (**G–I**).

In conclusion, we observed an increased number of TUNEL-positive oligodendrocytes in the white matter of the *twy/twy* mouse spinal cord that was subjected to progressive mechanical compression *vis a tergo* with aging, and the number of these cells increased with the magnitude of compression. Longitudinal topographic mapping of TUNEL-positive cells showed considerable distribution along the spinal cord axis. The results

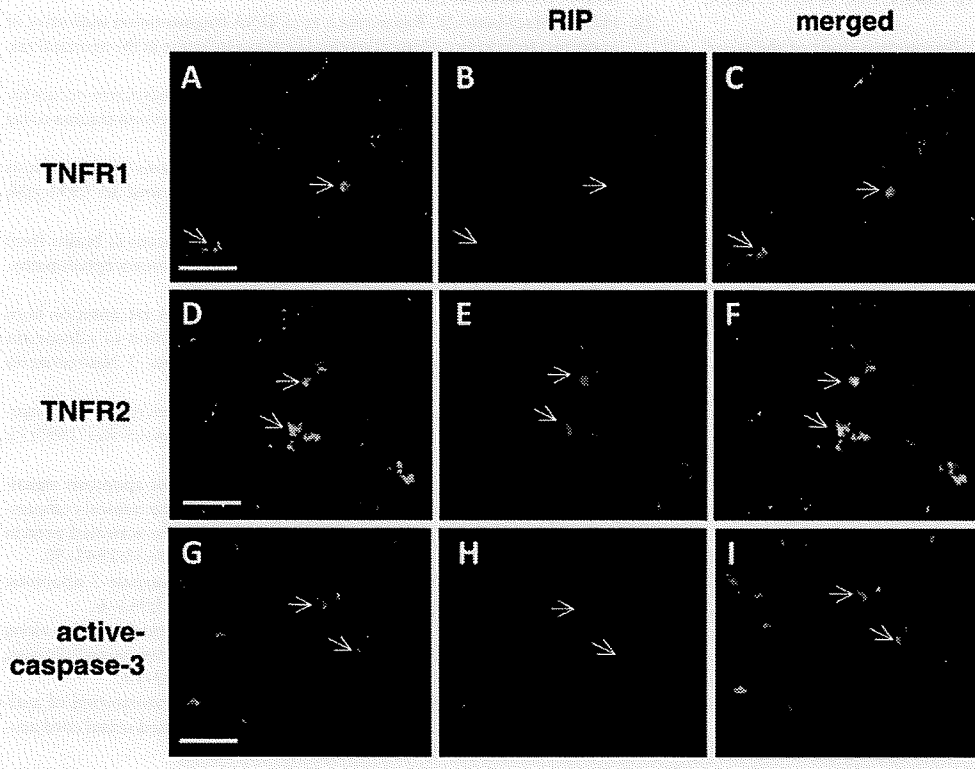

Figure 8. Photomicrographs showing double staining for TNFR1, TNFR2, and active-caspase-3 with immunoreactivity for oligodendrocyte RIP in the anterior funiculus at spinal cord level of maximal compression in *twy/twy* mice with severe compression. White arrows in **A–I**: colocalization of TNFR1, TNFR2, active-caspase-3 and RIP. Overlap of the markers appears yellow in the third rows. Note the expression of TNFR1, TNFR2, and active-caspase-3 in oligodendrocytes. Scale bars = 20 μm.

Copyright © Lippincott Williams & Wilkins. Unauthorized reproduction of this article is prohibited.